

# The role of Na<sub>v</sub>1.7 in human nociceptors: insights from human induced pluripotent stem cell–derived sensory neurons of erythromelalgia patients

Jannis E. Meents<sup>a</sup>, Elisangela Bressan<sup>a</sup>, Stephanie Sontag<sup>b,c</sup>, Alec Foerster<sup>a</sup>, Petra Hautvast<sup>a</sup>, Corinna Rösseler<sup>a</sup>, Martin Hampf<sup>a,d</sup>, Herdit Schüler<sup>e</sup>, Roman Goetzke<sup>f</sup>, Thi Kim Chi Le<sup>a</sup>, Inge Petter Kleggetveit<sup>g</sup>, Kim Le Cann<sup>a</sup>, Clara Kerth<sup>a</sup>, Anthony M. Rush<sup>h</sup>, Marc Rogers<sup>h</sup>, Zacharias Kohl<sup>i</sup>, Martin Schmelz<sup>j</sup>, Wolfgang Wagner<sup>b,f</sup>, Ellen Jorum<sup>g,k</sup>, Barbara Namer<sup>d</sup>, Beate Winner<sup>l</sup>, Martin Zenke<sup>b,c</sup>, Angelika Lampert<sup>a,\*</sup>

## Abstract

The chronic pain syndrome inherited erythromelalgia (IEM) is attributed to mutations in the voltage-gated sodium channel (Na<sub>v</sub>) 1.7. Still, recent studies targeting Na<sub>v</sub>1.7 in clinical trials have provided conflicting results. Here, we differentiated induced pluripotent stem cells from IEM patients with the Na<sub>v</sub>1.7/I848T mutation into sensory nociceptors. Action potentials in these IEM nociceptors displayed a decreased firing threshold, an enhanced upstroke, and afterhyperpolarization, all of which may explain the increased pain experienced by patients. Subsequently, we investigated the voltage dependence of the tetrodotoxin-sensitive Na<sub>v</sub> activation in these human sensory neurons using a specific prepulse voltage protocol. The IEM mutation induced a hyperpolarizing shift of Na<sub>v</sub> activation, which leads to activation of Na<sub>v</sub>1.7 at more negative potentials. Our results indicate that Na<sub>v</sub>1.7 is not active during subthreshold depolarizations, but that its activity defines the action potential threshold and contributes significantly to the action potential upstroke. Thus, our model system with induced pluripotent stem cell–derived sensory neurons provides a new rationale for Na<sub>v</sub>1.7 function and promises to be valuable as a translational tool to profile and develop more efficacious clinical analgesics.

**Keywords:** Erythromelalgia, Pain, Nociceptor, Induced pluripotent stem cells, Voltage-gated sodium channel, Action potential firing, Patch-clamp, iPS cells, Inherited pain syndrome

## 1. Introduction

About 10 years ago, patients were described with a complete loss of function of the voltage-gated sodium channel Na<sub>v</sub>1.7. These patients were unable to sense any pain, whereas other senses of the skin remained unaltered.<sup>9</sup> Shortly before, gain-of-function mutations in Na<sub>v</sub>1.7 in patients suffering from chronic pain syndromes, such as inherited erythromelalgia (IEM), had been identified.<sup>23,45</sup> These discoveries sparked hope for millions suffering from chronic pain: a new and promising drug target had emerged. Consequently, inhibitors of Na<sub>v</sub>1.7 were developed and some

entered clinical trials. Unfortunately, to date no, Na<sub>v</sub>1.7 inhibitors have shown significant clinical efficacy, and several have been given up (<https://clinicaltrials.gov>). Why are specific Na<sub>v</sub>1.7 inhibitors effective in heterologous systems and rodent models, but not in clinical trials? Our understanding is limited by the fact that it is difficult to investigate native human sensory neurons.

Recent recordings of postmortem dissociated human dorsal root ganglion (DRG) neurons suggest that Na<sub>v</sub>1.7 displays fundamentally different gating and pharmacological sensitivity to Na<sub>v</sub>1.7 inhibitors in human tissue compared with rodents or

Sponsorships or competing interests that may be relevant to content are disclosed at the end of this article.

J.E. Meents, E. Bressan, S. Sontag, and A. Foerster contributed equally to this work.

<sup>a</sup> Institute of Physiology, Medical Faculty, RWTH Aachen University, Aachen, Germany. Dr. Bressan is now with the German Center for Neurodegenerative Diseases (DZNE), Tübingen, Germany, <sup>b</sup> Department of Cell Biology, Institute for Biomedical Engineering, Medical Faculty, RWTH Aachen University, Aachen, Germany. Dr. Sontag is now with the Taconic Biosciences GmbH, Köln, Germany, <sup>c</sup> Helmholtz-Institute for Biomedical Engineering, RWTH Aachen University, Aachen, Germany, <sup>d</sup> Institute for Physiology and Pathophysiology, Friedrich-Alexander-University Erlangen-Nürnberg, Erlangen, Germany, <sup>e</sup> Institute of Human Genetics, Uniklinik RWTH Aachen, Aachen, Germany, <sup>f</sup> Division of Stem Cell Biology and Cellular Engineering, Helmholtz-Institute for Biomedical Engineering, RWTH Aachen University, Aachen, Germany, <sup>g</sup> Section of Clinical Neurophysiology, Department of Neurology, Oslo University Hospital-Rikshospitalet, Oslo, Norway, <sup>h</sup> Metrion Biosciences, Cambridge, United Kingdom, <sup>i</sup> Department of Molecular Neurology, Friedrich-Alexander-University Erlangen-Nürnberg, Erlangen, Germany, <sup>j</sup> Department of Experimental Pain Research Mannheim, Heidelberg University, Mannheim, Germany, <sup>k</sup> Institute of Clinical Medicine, University of Oslo, Oslo, Norway, <sup>l</sup> Department of Stem Cell Biology, Friedrich-Alexander-University Erlangen-Nürnberg, Erlangen, Germany

\*Corresponding author. Address: Institute of Physiology, Medical Faculty, RWTH Aachen University, Pauwelsstr 30, 52074 Aachen, Germany. Tel.: 0049 241 8088810; fax: 0049 241 8082434. E-mail address: [alampert@ukaachen.de](mailto:alampert@ukaachen.de) (A. Lampert).

Supplemental digital content is available for this article. Direct URL citations appear in the printed text and are provided in the HTML and PDF versions of this article on the journal's Web site ([www.painjournalonline.com](http://www.painjournalonline.com)).

PAIN 160 (2019) 1327–1341

Copyright © 2019 The Author(s). Published by Wolters Kluwer Health, Inc. on behalf of the International Association for the Study of Pain. This is an open-access article distributed under the terms of the Creative Commons Attribution-Non Commercial-No Derivatives License 4.0 (CCBY-NC-ND), where it is permissible to download and share the work provided it is properly cited. The work cannot be changed in any way or used commercially without permission from the journal.

<http://dx.doi.org/10.1097/j.pain.0000000000001511>

heterologous models.<sup>47</sup> It is generally assumed that subthreshold depolarizations that initiate action potentials are due to  $\text{Na}_v1.7$ -mediated ramp currents.<sup>12,21</sup> However, human DRG do not display such TTX-s ramp currents.<sup>47</sup> Based on experiments using knockout animals,  $\text{Na}_v1.7$  seems to contribute no more than 25% of the TTX-s current in sensory neurons.<sup>31</sup> Several studies have highlighted the differences between rodent and human nociceptors.<sup>13,20,35,37</sup> A recent report even suggests a role of  $\text{Na}_v1.7$  in regulation of gene expression, rather than in excitability.<sup>29</sup> Thus,  $\text{Na}_v1.7$  is a validated target for pain treatment in humans, and we need human translational models to assess gating and pharmacology of  $\text{Na}_v1.7$  in a physiological background.

The well-described IEM mutation  $\text{Na}_v1.7$  p.I848T<sup>45</sup> ( $\text{Na}_v1.7$ /I848T) induces a shift of voltage dependence of activation to hyperpolarized potentials in HEK cells.<sup>11,40,43</sup> This facilitates opening of the channel and has been linked to a reduced firing threshold and to an increased evoked firing frequency of rodent neurons.<sup>19</sup> Thus, in rodents, potentially painful symptoms could be explained intuitively. However, it is unclear whether these assumptions translate to human nociceptors.

In a previous study, induced pluripotent stem cell (iPS cell)-derived sensory neurons from a patient with the  $\text{Na}_v1.7$ /I848T mutation failed to show a significant increase in evoked firing frequency, although the neurons displayed a reduced action potential rheobase and expressed sodium currents sensitive to a potentially selective  $\text{Na}_v1.7$  inhibitor.<sup>5</sup> However, selectivity in native human tissue may be different.<sup>47</sup> Because no voltage-clamp experiments were conducted, the role of  $\text{Na}_v1.7$  is unclear, also if the IEM mutation induced a leftward shift of activation as suggested from heterologous expression systems. With this study, we aim to address these questions. We differentiated iPS cells from 2 related IEM patients (carrying  $\text{Na}_v1.7$ /I848T) into sensory neurons. We determined the voltage dependence of activation of the mutated  $\text{Na}_v1.7$  and how this affects action potential firing. Our results highlight the potential of this human model system for the development of new analgesic strategies.

## 2. Methods

### 2.1. Subjects

This study was conducted with iPS cells, derived from fibroblasts of 2 female subjects of the same family (mother and daughter, age at biopsy 59 and 36 years, respectively) clinically and genetically characterized with IEM.<sup>48</sup> The skin biopsies were obtained in Oslo, Norway, and fibroblast lines were generated at the University of Erlangen-Nürnberg following written informed consents of the patients (in Norwegian) with approval by the Institutional Review Board (Nr. 4120: “*Generierung von humanen neuronalen Modellen bei neurodegenerativen Erkrankungen*”), Department of Molecular Neurology, Universitätsklinikum Erlangen (Erlangen, Germany), and the local ethical committee South East Norway. Induced pluripotent stem cells derived from the 2 IEM patients are labelled IEM 1 (mother; EBiSC repository name UKAi0005-A) and IEM 2 (daughter; EBiSC repository name UKAi0006-A). HUES6 ES cells and iPS cells of healthy Caucasian non-IEM subjects (Ctrl 1, female, age 30 years, unpublished; Ctrl 2, female, age 3 years, previously referred to as iPS\_2<sup>33</sup>) were used as control. All experiments with human embryonic stem cells (HUES6) were performed in accordance with the German Stem Cell Act (RKI AZ.3.04.02/0085) and in the same manner as described below for iPS cells.

### 2.2. Generation and maintenance of induced pluripotent stem cells

Fibroblasts of IEM and Ctrl patients were reprogrammed into iPS cells using the CytoTune-iPS 2.0 Sendai Reprogramming Kit (Thermo Fisher Scientific, Schwerte, Germany) containing Sendai virus vectors for OCT4, KLF4, SOX2, and c-MYC. One day before transduction, fibroblasts were seeded at  $2 \times 10^4$  cells/cm<sup>2</sup> onto 0.1% gelatin-coated (Sigma-Aldrich, Taufkirchen, Germany) tissue culture plates and cultured in high-glucose DMEM, supplemented with 10% fetal calf serum, 100 U/mL penicillin, 100  $\mu$ g/mL streptomycin, and 2 mM L-glutamine (all Thermo Fisher Scientific). For transduction, 15  $\mu$ L of vector mix were applied and cells were cultured with virus particles for 2 days. On day 5 after transduction, fibroblasts were washed with 1 $\times$  phosphate-buffered saline (PBS; Thermo Fisher Scientific) and transferred onto irradiated mouse embryonic fibroblasts. After day 6, cells were cultured in KnockOut-DMEM (KO-DMEM) supplemented with 20% KnockOut serum replacement, 100 U/mL penicillin, 100  $\mu$ g/mL streptomycin, 2 mM L-glutamine, 0.1 mM nonessential amino acids (NEAA), 0.1 mM  $\beta$ -mercaptoethanol (all Thermo Fisher Scientific), and 10 ng/mL basic fibroblast growth factor (bFGF; PeproTech, Hamburg, Germany). Colonies were picked after 3 weeks. Induced pluripotent stem cells were maintained on Matrigel (Corning, Kaiserslautern, Germany) in mTeSR1 and passaged with dispase (both Stemcell Technologies, Cologne, Germany) every 5 to 6 days.

### 2.3. Sanger sequencing

Genomic DNA of iPS cells was isolated using the NucleoSpin Tissue Kit (Macherey-Nagel, Düren, Germany) according to the manufacturer's instructions.  $\text{Na}_v1.7$  target region was PCR-amplified with primers given in Supplementary Table S1 (available at <http://links.lww.com/PAIN/A749>). PCR products were purified with the NucleoSpin Gel and PCR Clean-up Kit (Macherey-Nagel) according to the manufacturer's instructions and sent for sequencing (Eurofins Genomics, Ebersberg, Germany).

### 2.4. Cytogenetic analysis

Structural and numerical chromosome alterations were investigated by conventional karyotyping using GTG banding at 400 to 550 band level. Metaphase spreads were prepared using standard procedures of blocking cell division at metaphase, hypotonic treatment, and methanol/acetic acid (3:1) fixation. GTG banding included trypsin pretreatment for partial removal of DNA-associated (chromosomal) proteins and subsequent Giemsa staining. Microscopy was performed using Axioplan fluorescence microscope (Carl Zeiss, Oberkochen, Germany) and IKARUS digital imaging systems (MetaSystems, Altlüßheim, Germany). On average, 20 GTG-banded metaphases were analysed per clone.

### 2.5. Embryoid body assay

To assess 3 germ layer differentiation potential, iPS cells were subjected to spontaneous differentiation as described previously.<sup>33</sup> Briefly, embryoid bodies were formed by 30 minutes of collagenase IV (Thermo Fisher Scientific) treatment, transferred to ultralow attachment plates (Corning), and grown in suspension with KO-DMEM supplemented with 20% fetal calf serum (Lonza, Basel, Switzerland), 100  $\mu$ M NEAA, 100 U/mL penicillin, 100  $\mu$ g/mL streptomycin, 2 mM L-glutamine, and 0.1 mM  $\beta$ -mercaptoethanol. Samples were harvested for RNA isolation on day 0, 7, 14, 17, and

21 of differentiation and analyzed for germ layer-specific genes by RT-qPCR.

## 2.6. Reverse transcription-quantitative PCR

RNA was isolated with the NucleoSpin RNA Kit (Macherey-Nagel) according to the manufacturer's instructions. RNA was reverse transcribed into cDNA using High-Capacity cDNA Reverse Transcriptase Kit (Thermo Fisher Scientific) or SensiFAST cDNA Synthesis Kit (Bioline, Luckenwalde, Germany). Quantitative PCR was performed on a StepOnePlus Real-Time cyler with FAST SYBR Green master mix (Thermo Fisher Scientific) or on a RotorGeneQ Real-Time cyler (Qiagen, Hilden, Germany) with SensiMix SYBR No-ROX Kit (Bioline). Human-specific primers (Eurofins Genomics) are listed in Supplementary Table S2 (available at <http://links.lww.com/PAIN/A749>). For heat maps (Supplementary Fig. S1c, available at <http://links.lww.com/PAIN/A749>), expression values were normalized per gene and subjected to bidirectional hierarchical clustering using Euclidean distance and average linkage clustering.

## 2.7. DNA methylation and Epi-Pluri-Score analysis

To validate successful reprogramming into pluripotent iPS cells, DNA methylation (DNAm) status of 3 CpG sites (cg22247240 in C14orf115, cg23737055 in ANKRD46, and cg13083810 in OCT4) was analyzed in stem cells as described previously.<sup>25</sup> In brief, genomic DNA was isolated and bisulfite-converted using the EZ DNA Methylation Kit (Zymo Research, Irvine, CA). The regions of interest were PCR-amplified using the PyroMark PCR Kit and pyrosequenced with gene-specific primers on a PyroMark Q96 ID instrument. DNAm at CpG sites was analyzed with the PyroMark CpG SW 1.0 software (all Qiagen). Methylation levels of CpG sites are characterized as  $\beta$  values with  $\beta$  value 0 and  $\beta$  value 1 representing 0% and 100% methylation, respectively. Epigenetic Pluripotency Score (Epi-Pluri-Score) was calculated as  $\beta$  value (ANKRD46) –  $\beta$  value (C14orf115) ranging from 1 for pluripotent cells to –1 for nonpluripotent (somatic) cells. In combination with the third CpG site in the pluripotency-associated gene OCT4, Epi-Pluri-Score classified all iPS cells and the HUES6 as pluripotent (see also Supplementary Fig. S1b, available at <http://links.lww.com/PAIN/A749>).

## 2.8. Differentiation into sensory neurons

Differentiation of stem cells was performed as described previously.<sup>7,16</sup> Induced pluripotent stem cells or HUES6 cells were seeded as single cells in a density of  $10^5$  cells/cm<sup>2</sup> in the presence of 10  $\mu$ M Y-27632 (Abcam Biochemicals, Bristol, United Kingdom). When cells reached 80% to 90% confluence, usually 24 hours after plating, we induced neural conversion using dual-SMAD inhibition.<sup>7</sup> LDN-193189 (100 nM; Sigma-Aldrich) and SB431542 (10  $\mu$ M; Miltenyi Biotec, Bergisch Gladbach, Germany) were added to the basal culture medium between days 0 to 5. To accelerate neural crest specification and peripheral neuron formation from neural crest cells, 3 small molecules (3  $\mu$ M CHIR99021, 10  $\mu$ M DAPT, and 10  $\mu$ M SU5402, all Tocris, Bristol, United Kingdom)<sup>7</sup> were added between days 2 to 10. Between days 0 and 5, cells were fed with knockout DMEM/F-12 containing 15% KnockOut serum replacement, 1 mM L-glutamine, 100  $\mu$ M NEAA, 100  $\mu$ M  $\beta$ -mercaptoethanol, 100 U/mL penicillin, and 100  $\mu$ g/mL streptomycin (all from Thermo Fisher Scientific). Between days 4 and 10, cells were fed with DMEM/F-12, containing 10 mL/l N2, 20 mL/l B27 minus vitamin A supplements, 100 U/mL

penicillin, and 100  $\mu$ g/mL streptomycin (all from Thermo Fisher Scientific). N2/B27 medium was added to basal medium at 25% between days 4 to 5, 50% between days 6 to 7, and 75% between days 8 to 10. On day 10, cells were dissociated using Accutase (Stemcell Technologies) and seeded on glass coverslips, coated with 50  $\mu$ g/mL poly-L-ornithine (Sigma-Aldrich) and 5  $\mu$ g/mL laminin (Thermo Fisher Scientific). From dissociation at differentiation day 10, neurons underwent a maturation period of 8 weeks in N2/B27 medium supplemented with 20 ng/mL NGF (R&D Systems, Minneapolis, MN), BDNF, GDNF (both from PeproTech), and 200 ng/mL ascorbic acid (Sigma-Aldrich). Medium was changed every 3 to 4 days.

## 2.9. Immunofluorescence imaging

For immunofluorescence staining, iPS cells or differentiated neurons were seeded onto glass cover slips, coated with Matrigel or poly-L-ornithin/laminin, respectively (Sigma-Aldrich and Thermo Fisher Scientific). Cells were fixed with 4% paraformaldehyde and blocked and permeabilized with 2% bovine serum albumin and 0.1% Triton X-100 in phosphate-buffered saline (all Sigma-Aldrich). Induced pluripotent stem cells were stained with anti-OCT4 (clone sc-9081; Santa Cruz Biotechnology, Dallas, TX) and anti-TRA-1-60 (clone TRA-1-60; Merck Millipore, Darmstadt, Germany) (Supplementary Fig. S1a, available at <http://links.lww.com/PAIN/A749>). Induced pluripotent stem cell-derived neurons were stained with anti-peripherin (clone sc-7604; Santa Cruz Biotechnology), anti- $\beta$ -III-tubulin (clone TUJ-1; R&D Systems), anti-Na<sub>v</sub>1.8 (clone ASC-016, 1:1000, see Supplementary Fig. S2, available at <http://links.lww.com/PAIN/A749>), and anti-TRPV1 (clone ACC-030, 1:1000; all from Alomone Labs, Jerusalem, Israel). Secondary antibodies were goat anti-rabbit IgG Alexa Fluor 594 (OCT4, Na<sub>v</sub>1.8, TRPV1), donkey anti-mouse IgM Alexa Fluor 488 (TRA-1-60), donkey anti-goat IgG Alexa Fluor 488 (peripherin), and goat anti-mouse IgG Alexa Fluor 488 and 594 ( $\beta$ -III-tubulin). Nuclei were counterstained with DAPI (all Thermo Fisher Scientific). Fluorescent images were acquired using an LSM 700 confocal microscope (Carl Zeiss) with 40 $\times$  oil-immersion objective, 4 $\times$  line averaging, 200 mHz scanning speed, and pinhole set to 1 Airy unit. Fluorescent images were obtained on maturation day M35.

## 2.10. Calcium imaging

Stem cell-derived sensory neurons were loaded with Fura-2 AM (5  $\mu$ M; Biotium, Scarborough, Canada), supplemented with Pluronic F-127 (0.04%; Thermo Fisher Scientific), for 30 minutes followed by 15 minutes washout at 37°C and 5% CO<sub>2</sub>. Experiments were performed at room temperature using a Till Photonics Polychrome V monochromator (excitation wavelengths 340/380 nm) and were recorded using a 12-bit CCD camera (Imago Sensicam QE; Till Photonics, Gräfeling, Germany) at 1 Hz and an exposure time of 50 ms. The fluorescence ratio was calculated for all regions of interest after background subtraction (TILLvision 4.0.1.3 software, Till Photonics). Cells were continuously superfused through a gravity-driven perfusion system. Extracellular solution was composed of (in mM): 145 NaCl, 5 KCl, 1.25 CaCl<sub>2</sub>, 1 MgCl<sub>2</sub>, 10 HEPES, and 10 glucose (pH 7.4). For a solution containing 60 mM KCl, the extracellular solution was prepared by reducing NaCl to 90 mM. Capsaicin (1  $\mu$ M), AITC (100  $\mu$ M), menthol (100  $\mu$ M) (all from Sigma-Aldrich), pH 6.0, and high KCl solution (60 mM) were diluted in extracellular solution and applied for 30 seconds each at an interval of 5 minutes. Calcium imaging was performed on maturation day M35.



### 2.11. Electrophysiology

Whole-cell patch-clamp recordings were performed on iPS cell-derived neurons after a minimum of 8 weeks of maturation. Experiments were performed using a HEKA EPC 10USB amplifier and PatchMaster and analyzed using FitMaster v2.8 software (all HEKA electronics, Lambrecht, Germany), Igor Pro (WaveMetrics, Portland, OR), and GraphPad Prism version 5 or 6 (GraphPad Software, Inc, La Jolla, CA). Series resistance was compensated by 65% to 85%. Currents were low-pass filtered at 10 kHz and sampled at 100 kHz. Leak current was subtracted using the P/4 method. The liquid junction potential was not corrected. All experiments were performed at room temperature.

### 2.12. Current-clamp recordings

The following bath solution was used (in mM): 140 NaCl, 3 KCl, 1 MgCl<sub>2</sub>, 1 CaCl<sub>2</sub>, 10 HEPES, and 20 glucose (pH 7.4; 300–310 mOsm). Intracellular solution contained (in mM): 4 NaCl, 135 K-gluconate, 3 MgCl<sub>2</sub>, 5 EGTA, 5 HEPES, 2 Na<sub>2</sub>-ATP, and 0.3 Na-GTP (pH 7.25; 290–300 mOsm). The resting membrane potential (RMP) was measured immediately after establishing the whole-cell configuration. Holding current was then adjusted to achieve a membrane voltage of  $-70 \pm 5$  mV. Action potentials were induced by slow ramp current injections (from 0 to 500 pA in 400 ms) and subsequently by 500 ms square current injections in steps of  $0.5 \times$  rheobase stimulus (up to  $5.5 \times$  rheobase stimulus). Action potentials were only considered if they exceeded 0 mV. The first action potential evoked by the square pulse protocol was used to calculate the action potential properties. The threshold was defined as the minimum of the first derivative of the action potential (=the point of inflection during the depolarization). The afterhyperpolarization is the minimum after the action potential peak. The amplitude is measured between RMP and action potential peak. To calculate the action potential half-width, the half-distance between threshold and peak is taken and the distance between this point during depolarization and repolarization is measured. The time to peak is the duration between current pulse onset and action potential peak. The maximum slope of the upstroke was calculated between threshold and peak, whereas the slope of the subthreshold depolarization was determined between RMP and threshold. Current-clamp recordings were performed between maturation days 55 and 75. For the characterization of action potential properties, data from the 2 IEM clones (IEM 1 and IEM 2) as well as data from the 2 control clones (Ctrl 1 and Ctrl 2) were pooled.

### 2.13. Voltage-clamp recordings

External solution contained (in mM): 140 NaCl, 1 MgCl<sub>2</sub>, 1 CaCl<sub>2</sub>, 10 HEPES, 1 glucose, 20 TEA-Cl, 1 4-aminopyridin, and 0.1 CdCl<sub>2</sub> (pH 7.4; 300–310 mOsm), and the internal solution contained (in mM): 140 CsF, 10 NaCl, 10 HEPES, 1 EGTA, 5 glucose, and 5 TEA-Cl (pH 7.3; 290–300 mOsm). Five hundred nM TTX (Tocris Bioscience) was diluted in external solution and applied through a gravity-driven perfusion system. For voltage clamp, 40 ms voltage pulses from  $-80$  mV to  $+40$  mV were applied from a holding potential of  $-120$  mV to acquire current–voltage curves. To isolate somatic currents and avoid space clamp artefacts, a voltage prepulse protocol was used to inactivate distant sodium channels as previously described<sup>28</sup> (see Results). The prepulse (4–6 ms,  $-50$  to  $-15$  mV) was followed by a repolarizing interpulse (1 ms,  $-120$  to  $-70$  mV), which preceded the regular testpulse (see Fig 4a) (40 ms,  $-80$  to  $+40$  mV

in 10 mV steps). Prepulse and interpulse voltage and duration were adjusted to each cell individually to eliminate all artefacts and obtain optimal voltage-clamp conditions. Subsequently, 500 nM TTX was applied, and the identical voltage pulse protocol was repeated. Currents measured after TTX application were considered to be TTX-resistant (TTX-r). TTX-r current traces were subtracted from current traces measured before TTX application to obtain the TTX-sensitive (TTX-s) component. Conductance (G) was calculated at each voltage (V) using the equation  $G = I/(V - V_{rev})$ , where  $V_{rev}$  is the reversal potential, determined for each cell individually. Normalized conductance–voltage curves were fitted with a Boltzmann equation:  $G/G_{max} = G_{max}/(1 + \exp[(V - V_{1/2})/k])$ , where  $G_{max}$  is the maximum conductance, V is the membrane voltage,  $V_{1/2}$  is the voltage at half-maximal channel activation, and k is the slope factor.

Voltage-clamp experiments to determine the block induced by ProTx-II were performed in self-made HEK293 cell lines, stably expressing hNav1.7 or hNav1.6. External solution for HEK293 cells contained (in mM): 140 NaCl, 3 KCl, 1 MgCl<sub>2</sub>, 1 CaCl<sub>2</sub>, 10 HEPES, and 20 glucose (pH 7.4, 310 mOsm). The internal solution for HEK293 cells consisted of (in mM): 10 NaCl, 140 CsF, 1 EGTA, 10 HEPES, and 18 sucrose (pH 7.33, 305 mOsm). Solutions containing ProTx-II (Smartox Biotechnology, Saint Martin d'Hères, France) were prepared on the same experimental day. The toxin was diluted to a final concentration of 10 nM (HEK293) or 5 nM (iPS cells) in external solution and adding 0.1% BSA (Sigma-Aldrich). Stock solutions of ProTx-II (20  $\mu$ M) dissolved in H<sub>2</sub>O were stored at  $-20^{\circ}\text{C}$ . Voltage-clamp recordings were performed between maturation days 55 and 70.

### 2.14. Statistical analysis

Statistical analysis was performed using GraphPad Prism version 5 or 6 (GraphPad Software, Inc). Two groups were compared using a 2-tailed *t* test or a Mann–Whitney test, depending on normal distribution. Comparisons between 3 or more groups were performed using a 1-way analysis of variance followed by Bonferroni multiple comparisons test. Statistical information, including the tests used, is presented in the figure legends. The exact value of n (representing number of cells) can be found in the figure legends. For voltage-clamp data, values of n are presented in **Table 1**. Data are presented as mean  $\pm$  SEM. *P* values  $<0.05$  were considered significant. The following significance values are given \**P*  $< 0.05$ ; \*\**P*  $< 0.01$ ; \*\*\**P*  $< 0.001$ . No outliers were defined or eliminated.

### 2.15. Data availability

Inherited erythromelalgia patient-derived iPS cells will be entered into the European Bank for induced pluripotent Stem Cells (www.EbiSC.org) by the names UKAi0006-A (IEM 1) and UKAi0007-A (IEM 2). The data that support the findings of this study are available from the corresponding author on request.

## 3. Results

### 3.1. Sensory neurons are derived from erythromelalgia-specific induced pluripotent stem cells

Induced pluripotent stem cells were generated from fibroblasts of 2 consanguineous IEM patients using nonintegrating Sendai virus vectors. Patients (mother and daughter) were heterozygous for the I848T mutation in Na<sub>v</sub>1.7<sup>48</sup> and iPS cells are referred to as IEM 1 and IEM 2 for the mother and the daughter, respectively

(Figs. 1A and B). Induced pluripotent stem cells were pluripotent by morphology, expression of pluripotency markers, and Epi-Pluri-Score (Supplementary Fig. S1a–c, available at <http://links.lww.com/PAIN/A749>). In addition, iPS cells demonstrated a normal karyotype and were heterozygous for the I848T mutation (Supplementary Fig. S1d and e, available at <http://links.lww.com/PAIN/A749>). HUES6 embryonal stem cells (ES cells) and iPS cells of healthy Caucasian non-IEM subjects (Ctrl 1 and Ctrl 2<sup>33</sup>) were used as control.

All iPS cell clones were differentiated into sensory neurons using small molecule inhibition<sup>7,16</sup> for 10 days, followed by maturation using neuronal growth factors for a minimum of 8 weeks (Fig. 2A). Differentiated neurons formed dense neuronal networks, large ganglion-like structures, and stained positive for specific neuronal markers, such as the peripheral nervous system type III filament protein peripherin and the class III  $\beta$ -tubulin TUJ-1 (Fig. 2B). Neurons also expressed the sensory neuron-specific ion channels  $Na_v1.8$  and TRPV1 (Figs. 2C and D).

To also functionally characterize iPS cell-derived and ES cell-derived neurons, expression of transient receptor potential channels and acid-sensing ion channels, which are primarily expressed in sensory neurons and are important for sensing heat, cold, and chemical stimuli, was analyzed by calcium imaging using specific agonists (Fig. 2E; and Supplementary Fig. S3, available at <http://links.lww.com/PAIN/A749>). The large majority of IEM 1 and IEM 2 iPS cell-derived neurons responded to pH 6 stimulation, indicating the expression of acid-sensing ion channels. A smaller cell fraction responded to menthol, AITC, or capsaicin, indicating the functional presence of TRPM8, TRPA1, and TRPV1, respectively. To test for functional expression of sensory neuron-specific  $Na_v$  channels, we performed whole-cell voltage-clamp experiments using  $Na_v$ -specific blockers. Recordings during application of tetrodotoxin (TTX, 500 nM) show a prominent TTX-resistant (TTX-r) current, indicating the functional expression of  $Na_v1.8$  and potentially  $Na_v1.9$  (Fig. 2F and Table 1). In addition, application of the  $Na_v1.7$ -specific blocker ProTx-II (5 nM) led to a clear reduction in inward current ( $25 \pm 7\%$ ;  $n = 4$ ), indicating the functional expression of  $Na_v1.7$  (Fig. 2G). The latter was corroborated by real-time qPCR experiments

(Supplementary Fig. S4, available at <http://links.lww.com/PAIN/A749>).

Taken together, these results demonstrate that functional sensory neurons can be generated from IEM-specific iPS cells.

### 3.2. Action potential threshold is reduced for erythromelalgia nociceptors

Based on experiments in rodent sensory neurons, the  $Na_v1.7$ /I848T mutation has been suggested to induce pain in patients by depolarizing the RMP of nociceptors, lowering the action potential threshold, and increasing action potential firing.<sup>19</sup> However, a more recent study did not fully reproduce this predicted phenotype in human iPS cell-derived sensory neurons.<sup>5</sup> To clarify the effect of the mutation in a human system, iPS cell-derived sensory neurons from IEM and control patients (in the following referred to as IEM nociceptors and controls) were used for whole-cell current-clamp electrophysiology (Fig. 3A). We found the RMP to be slightly but not significantly hyperpolarized in IEM nociceptors (Fig. 3B). The measured RMP was generally more depolarized than what had previously been found in iPS cell-derived peripheral neurons of IEM patients,<sup>5</sup> but was comparable with the RMP of mouse peripheral sensory neurons and of iPS cell-derived human central and peripheral neurons from healthy individuals.<sup>3,32,39,42</sup> The action potential threshold was significantly reduced in neurons from IEM patients (Fig. 3C), suggesting an increased excitability of these cells. In addition, we found single action potential characteristics to be affected by the mutation: the hyperpolarization that follows each action potential was more pronounced in IEM nociceptors (Fig. 3D), potentially explaining the faster conduction of active C-fiber nociceptors measured previously in an IEM patient with the identical mutation<sup>30</sup> (see Discussion). In addition, IEM nociceptors showed an increase in action potential amplitude (Fig. 3E), suggesting more synchronized activity of different  $Na_v$  isoforms and indicating that IEM nociceptors generate a stronger depolarization during the action potential.

These results suggest that  $Na_v1.7$  plays an important role not only in setting the action potential threshold but also during the

**Table 1**  
**Voltage-clamp properties of iPS cell-derived nociceptors.**

	IEM 1	IEM 2	IEM 2 + ProTx-II	Ctrl 1	Ctrl 2	Ctrl 2 + ProTx-II
Cell capacitance (pF)	30.2 $\pm$ 2.7	48.4 $\pm$ 7.4	50.9 $\pm$ 6.2	20.4 $\pm$ 1.8	41.05 $\pm$ 4.9	43.4 $\pm$ 9.4
Prepulse (mV)	-37 $\pm$ 2	-34 $\pm$ 2	-37 $\pm$ 2	-27 $\pm$ 2	-28 $\pm$ 1	-36 $\pm$ 2
n	25	21	14	9	23	14
TTX-s current						
Current density (pA/pF)	173 $\pm$ 15	151 $\pm$ 25	127 $\pm$ 13	88 $\pm$ 24	116 $\pm$ 14	141 $\pm$ 17
$V_{1/2}$ (mV)	-24.4 $\pm$ 1.8	-24.7 $\pm$ 1.1	-26.8 $\pm$ 1.1	-17.6 $\pm$ 1.6	-18.7 $\pm$ 1.1	-25.3 $\pm$ 1.9
Slope (mV)	6.6 $\pm$ 0.3	6 $\pm$ 0.3	5.7 $\pm$ 0.4	6.6 $\pm$ 0.5	6.1 $\pm$ 0.3	5.9 $\pm$ 0.3
n	20	20	13	9	21	12
Total current						
Current density (pA/pF)	175 $\pm$ 16	162 $\pm$ 27	145 $\pm$ 13	95 $\pm$ 29	126 $\pm$ 16	151 $\pm$ 18
$V_{1/2}$ (mV)	-26.5 $\pm$ 1.8	-24.4 $\pm$ 1.2	-26.8 $\pm$ 1.1	-17 $\pm$ 1.8	-18.9 $\pm$ 1.1	-25.9 $\pm$ 1.7
Slope (mV)	6.9 $\pm$ 0.2	6.2 $\pm$ 0.2	5.9 $\pm$ 0.2	6.6 $\pm$ 0.4	6.6 $\pm$ 0.4	6.4 $\pm$ 0.3
n	25	21	14	8	23	14
TTX-r current						
Current density (pA/pF)	38 $\pm$ 5	36 $\pm$ 12	82 $\pm$ 42	n/a	40 $\pm$ 7	60 $\pm$ 19
$V_{1/2}$ (mV)	-31.3 $\pm$ 2.5	-32.9 $\pm$ 4.7	-28.9 $\pm$ 2.4	n/a	-30.6 $\pm$ 1.5	-29.9 $\pm$ 2.6
Slope (mV)	8.7 $\pm$ 0.8	6.9 $\pm$ 0.8	9 $\pm$ 1.4	n/a	9.1 $\pm$ 1.1	7.8 $\pm$ 0.6
n	11	7	4	0	9	7

IEM, inherited erythromelalgia; iPS, induced pluripotent stem.

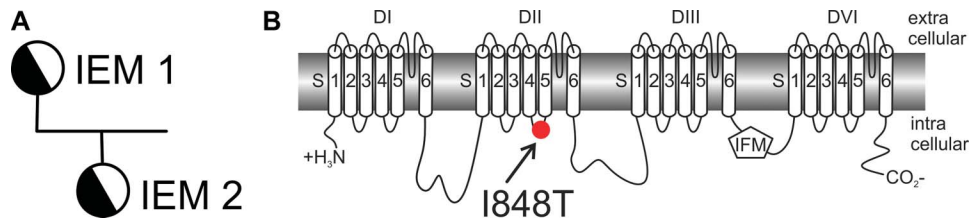


**Figure 1.**  $Na_V1.7/I848T$  mutation in IEM patients. (A) Segregation of  $Na_V1.7/I848T$  mutation in IEM study subjects. IEM 1, mother; IEM 2, daughter; both previously investigated in Ref. 48. (B) Location of the I848T mutation in the  $Na_V1.7$  channel protein. IEM, inherited erythromelalgia.

upstroke of the action potential. Accordingly, IEM nociceptors had a reduced action potential half-width (Fig. 3F), a reduced time-to-peak of the action potential (Fig. 3G), and a steeper slope of the upstroke (Fig. 3H). However, the slope of the subthreshold depolarization did not differ between IEM and control nociceptors (Fig. 3I), indicating that  $Na_V1.7$  may not play a major role during human subthreshold depolarizations, as suggested before<sup>47</sup> but in contrast to findings in rodents.<sup>13</sup>

Most of the changes we observed in action potential characteristics of IEM nociceptors might support higher frequency firing. We therefore compared the evoked action potential firing frequency in response to increasing current injections (Fig. 3J). Although IEM nociceptors seemed to support higher frequency firing, there was considerable variability between cells from the same or different clones, making these data unsuitable for statistical comparison. We find a slight increase in tonic action potential firing in IEM nociceptors compared with Ctrl neurons (Supplementary Fig. S5, available at <http://links.lww.com/PAIN/A749>).

### 3.3. A prepulse voltage protocol allows for accurate measurements of $Na_V$ voltage dependence in human sensory neurons

The reduced action potential threshold in IEM nociceptors could be indicative of a shift in voltage dependence of activation in the mutated  $Na_V1.7/I848T$ , as suggested by recordings in heterologous expression systems.<sup>11,40</sup> However, it is not known whether this shift is also present in human nociceptors. So far, IEM-related changes in voltage dependence of  $Na_V$  activation have not been investigated in human sensory neurons. These data are, however, crucial to determine whether the predictions based on heterologous model systems are even clinically relevant in the patient, and whether they pave the way to the correct pharmacological targets.

We investigated the voltage dependence of activation of  $Na_V1.7$  in IEM and control nociceptors using whole-cell voltage-clamp electrophysiology. Because iPS cell-derived nociceptors were grown for 8 weeks to obtain mature neurons, these cells had grown extensive neurite networks. Such neurons are notoriously difficult to use for voltage-clamp recordings due to space clamp artefacts and distortion of the current recording by unwanted activation of peripheral sodium channels. We therefore applied a prepulse voltage protocol, specifically adjusted to each cell, to inactivate and therefore eliminate unwanted peripheral sodium channel input<sup>28</sup> (Fig. 4A). This protocol allowed for accurate recording of somatic sodium channel activation (Fig. 4B) without space clamp artefacts. Varying prepulse voltages have no effect on voltage dependence of activation of WT  $Na_V1.7$  (Supplementary Fig. S6, available at <http://links.lww.com/PAIN/A749>).

Apart from  $Na_V1.7$ , it has been shown that human nociceptors also express  $Na_V1.1$ , 1.2, 1.3, 1.6, 1.8, and 1.9.<sup>5</sup> After measuring

the total whole-cell current (Fig. 4B), we applied the  $Na_V$  inhibitor TTX (500 nM) to measure the TTX-resistant (TTX-r) current component, which is mainly mediated by  $Na_V1.8$  and 1.9 (Fig. 4C). We recorded TTX-r current in all groups apart from Ctrl 1 nociceptors (Table 1) where expression of TTX-r channels seems to be decreased. During data analysis, the TTX-r component was subtracted from the total current to obtain the  $Na_V1.7$ -containing TTX-sensitive (TTX-s) current component (Figs. 4D and E). Because  $Na_V1.7$  is one of the predominant TTX-s isoforms in peripheral sensory neurons, we used this TTX-s voltage dependence to measure the effect of the IEM mutation in human iPS cell-derived nociceptors. Finally, recordings done without this prepulse protocol show clear signs of inaccurate voltage clamp with space clamp artefacts (Fig. 4F).

### 3.4. The erythromelalgia mutation shifts the voltage dependence of activation to more hyperpolarized potentials

We used the specific prepulse voltage protocol to measure accurately clamped TTX-s whole-cell currents in control and IEM nociceptors (Fig. 5A). The TTX-s current–voltage relationship (Fig. 5B) was used to determine the voltage dependence of activation of all TTX-s channels (Fig. 5C). If the IEM mutation does indeed induce a shift in voltage dependence of  $Na_V1.7$ , this should become apparent in the TTX-s activation curve. Activation curves from the 2 healthy control patients were almost identical with a  $V_{1/2}$  of  $-17.6$  mV (Ctrl 1) and  $-18.7$  mV (Ctrl 2). By contrast, nociceptors from the 2 patients carrying the  $Na_V1.7/I848T$  mutation showed a hyperpolarized activation curve, with a  $V_{1/2}$  of  $-24.4$  mV (IEM 1) and  $-24.7$  mV (IEM 2) (Table 1 and Figs. 5C and D). This 6.4 mV shift in voltage dependence of activation can explain the lowered action potential threshold seen in current-clamp recordings and the increased pain experienced by the patients. No significant differences were found in the slope of the activation curve or in TTX-s current density (Table 1 and Fig. 5E).

A similar hyperpolarized shift was also apparent in the total current before subtraction of TTX-r currents (Figs. 5F and G), indicating that  $Na_V1.7$  plays an important role in setting the voltage dependence of activation of the neuron. When we analyzed the TTX-r current component, we observed no difference in voltage dependence of activation between IEM and control nociceptors (Fig. 5H), confirming that the hyperpolarizing shift is restricted to the TTX-s current component. It also underlines the important role of  $Na_V1.7$  because the hyperpolarized shift in the total current is not compensated or masked by TTX-r channel activity. In analyzing the TTX-r current, we noticed a shallower slope of the activation curves in all measured groups compared with the total and the TTX-s currents (Table 1 and Fig. 5H). This could be due to an overlay of very hyperpolarized and very depolarized curves and might therefore reflect considerable differences in voltage dependence of  $Na_V1.8$  and 1.9.



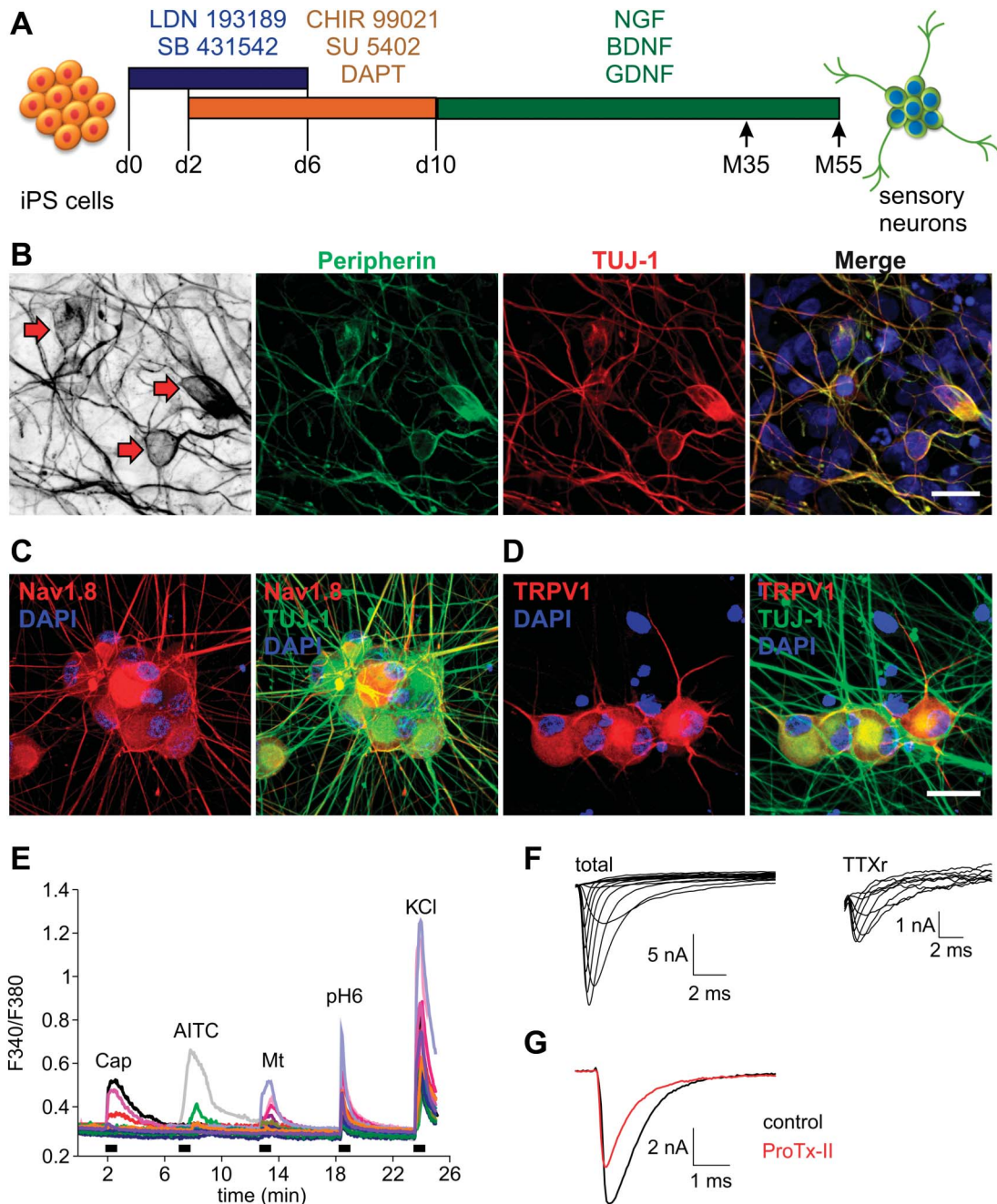


**Figure 2.** Functional sensory neurons are generated from iPS cells. (A) Differentiation scheme of iPS cells into sensory neurons with dual-SMAD inhibition (LDN193189 and SB431542), VEGF/FGF/PDGF inhibition (SU5402), Notch inhibition (DAPT), and WNT activation (CHIR99021) for 10 days (d0–d10), followed by growth factor (NGF, BDNF, and GDNF)-driven neuron maturation for 8 weeks. On maturation day M35 and M55, neurons were used for analysis. (B) Representative phase-contrast and immunofluorescence images of iPS cell-derived neurons expressing peripherin (green) and TUJ-1 (red) of IEM 1. Scale bar 100  $\mu$ m. (C and D) Representative immunofluorescence images of neurons from IEM 1 stained positive for  $\text{Na}_v1.8$  (C) (see also Supplementary Fig. S2, available at <http://links.lww.com/PAIN/A749>) and TRPV1 (D) (both red) and TUJ-1 (green). Nuclei were counterstained with DAPI (blue). Scale bar 100  $\mu$ m. (E) Representative calcium imaging recording performed on iPS cell-derived neurons from clone IEM 1. Neurons were stimulated with capsaicin (1  $\mu$ M), AITC (100  $\mu$ M), menthol (100  $\mu$ M), pH 6.0, and KCl (60 mM) for 30 seconds each as indicated. Response profiles of 18 cells are overlaid. For quantification, see Supplementary Figure S3 (available at <http://links.lww.com/PAIN/A749>). (F) Representative recording of an IEM 1 neuron. Traces display the neuron's total (left) and TTX-r (right) currents, showing functional expression of TTX-r  $\text{Na}_v$  channels. See also Table 1. (G) Representative recording of an IEM 1 neuron, showing functional expression of  $\text{Na}_v1.7$ . Total  $\text{Na}_v$  current is shown before (black) and after (red) 20 minutes of application of the  $\text{Na}_v1.7$ -specific blocker ProTx-II (5 nM). Data shown in (B–E) were gathered on maturation day M35. IEM, inherited erythromelalgia; iPS cell, induced pluripotent stem cell.

### 3.5. Erythromelalgia-induced shift of activation is abolished by application of ProTx-II

We next sought to determine whether the hyperpolarized shift of activation, seen in IEM nociceptors, is indeed due to  $\text{Na}_v1.7$  because the TTX-s currents measured above are still a combination of  $\text{Na}_v1.7$  and other  $\text{Na}_v$  isoforms. The tarantula toxin ProTx-II has been described as a sodium channel-blocking peptide with  $\sim$ 100-fold

selectivity to  $\text{Na}_v1.7$  compared with other  $\text{Na}_v$  isoforms.<sup>27,38</sup> We tested ProTx-II in HEK293 cells, expressing either  $\text{Na}_v1.7$  or  $\text{Na}_v1.6$  (Fig. 6A), which had been described as having the second-highest affinity to the compound.<sup>38</sup> In our hands, ProTx-II (10 nM) blocked  $57 \pm 6\%$  of the  $\text{Na}_v1.7$ -mediated current (Fig. 6B) with a very slow time course, not having reached a steady state after 10 minutes. ProTx-II-mediated block of  $\text{Na}_v1.6$  current, however, was

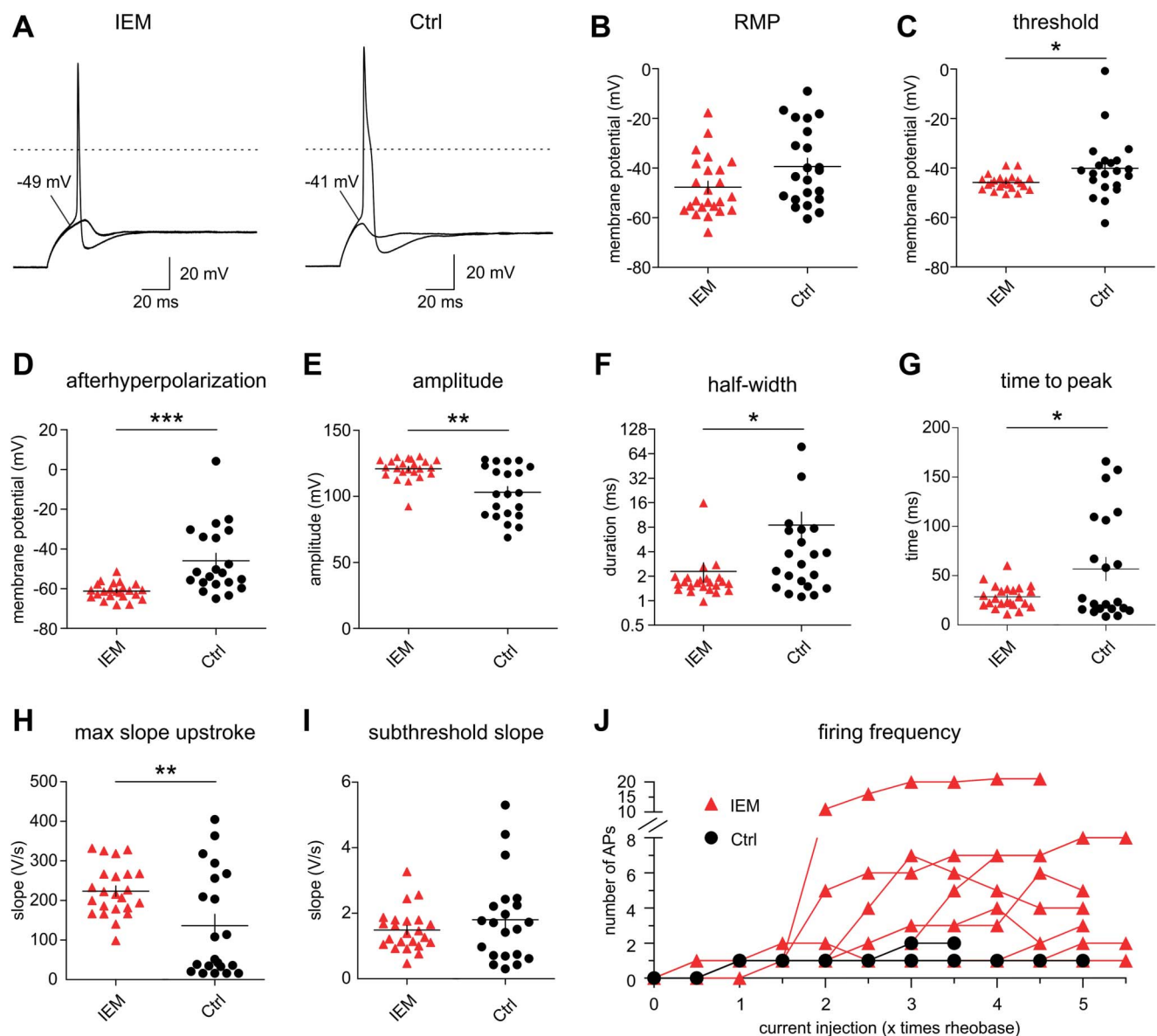


**Figure 3.** The IEM mutation changes action potential characteristics. (A) Representative action potentials recorded in IEM 2 (left) and Ctrl 2 (right) nociceptors. Action potential thresholds for each particular neuron are indicated. Dotted line represents 0 mV. (B) The RMP was  $-47.7 \pm 2.4$  mV for IEM and  $-39.3 \pm 3.3$  mV for Ctrl nociceptors ( $n = 24$  and  $22$ ;  $P = 0.05$  unpaired  $t$  test;  $t = 2.07$ ,  $df = 44$ ). (C) The action potential threshold was significantly lowered in IEM nociceptors ( $-45.9 \pm 0.6$  mV in IEM and  $-40.1 \pm 2.8$  mV in Ctrl;  $n = 23$  and  $21$ ;  $P = 0.02$ , Mann–Whitney test). (D) IEM nociceptors display a stronger hyperpolarization after each action potential ( $-61.2 \pm 0.8$  mV for IEM and  $-45.9 \pm 3.7$  mV for Ctrl;  $n = 23$  and  $21$ ;  $P < 0.0001$ , Mann–Whitney test). (E) IEM action potentials had a mean amplitude of  $120.9 \pm 1.7$  mV, compared with  $103.1 \pm 4.3$  mV in Ctrl nociceptors ( $n = 23$  and  $21$ ;  $P = 0.004$ , Mann–Whitney test). (F) Action potentials in IEM nociceptors had a mean half-width of  $2.3 \pm 0.6$  ms, compared with  $8.5 \pm 3.8$  ms in Ctrl nociceptors ( $n = 23$  and  $21$ ;  $P = 0.02$ , Mann–Whitney test). (G) The time from pulse onset to the action potential peak is significantly shorter in IEM nociceptors ( $28.6 \pm 2.4$  ms, compared with  $56.8 \pm 11.8$  ms in Ctrl;  $n = 23$  and  $21$ ;  $P = 0.019$ , unpaired  $t$  test;  $t = 2.44$ ,  $df = 42$ ). (H) Nociceptors for IEM patients have a steeper maximum slope of the action potential upstroke ( $223.7 \pm 13.2$  V/s, compared with  $136.3 \pm 29$  V/s in Ctrl;  $n = 23$  and  $21$ ;  $P = 0.007$ , unpaired  $t$  test;  $t = 2.83$ ,  $df = 42$ ). (I) The slope of the subthreshold depolarization is not different between IEM and Ctrl nociceptors ( $1.5 \pm 0.1$  V/s for IEM vs  $1.8 \pm 0.3$  V/s for Ctrl;  $n = 23$  and  $21$ ;  $P = 0.8$ , Mann–Whitney test). (J) Action potential (AP) frequency induced by increasing stepwise current injections ( $n = 14$  for IEM and  $n = 5$  for Ctrl; note that some traces are overlaid). None of the measured Ctrl nociceptors fired more than 2 action potentials. The current injection protocol is identical to the one in Supplementary Fig. S5b (available at <http://links.lww.com/PAIN/A749>). Neurons were held at an RMP around  $-70$  mV and depolarized by square current injections in steps of  $0.5 \times$  rheobase to evoke action potential firing. IEM, inherited erythromelalgia; RMP, resting membrane potential.

not significant compared with vehicle measurements (Figs. 6A and B).

The slow time course of the  $\text{Na}_v1.7$  block made the drug unsuitable for perfusion-driven application on iPS cell-derived nociceptors while measuring voltage dependence of activation. We therefore added ProTx-II in an even more  $\text{Na}_v1.7$ -specific concentration (5 nM, Fig. 2G) to the bath solution and performed recordings on IEM 2 and Ctrl 2 nociceptors because these had

shown prominent TTX-r currents. The following recordings were performed as described above, including application of TTX. This procedure allowed for measuring the TTX-s but  $\text{Na}_v1.7$ -free current component (Fig. 6C), which should be identical between IEM and control nociceptors. Indeed, voltage dependence of activation was found to be indistinguishable between IEM 2 and Ctrl 2 (Figs. 6C and D and Table 1). This confirms that the observed shift in voltage-dependent gating is indeed mediated by



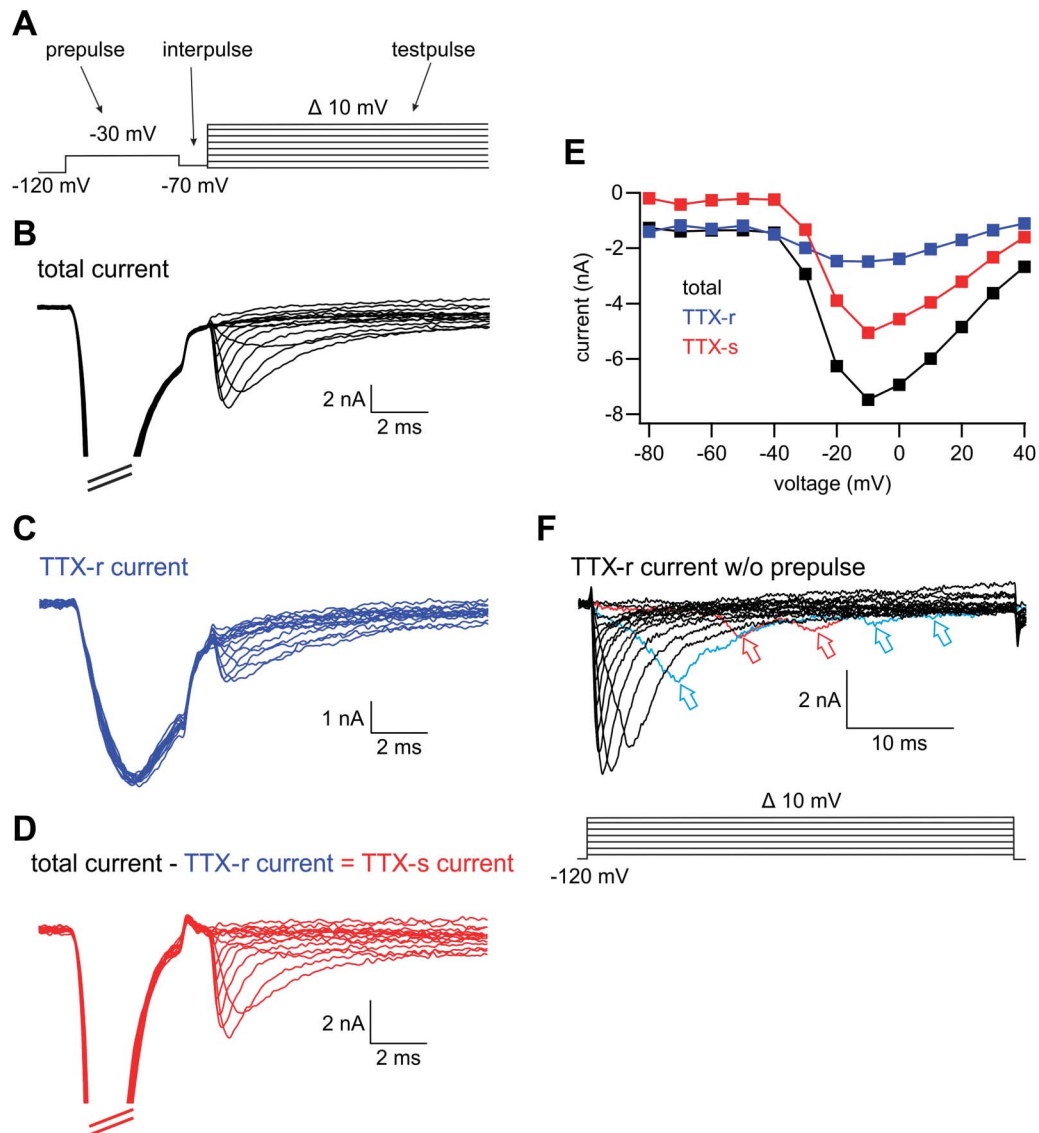


**Figure 4.** Voltage-clamp protocol to measure TTX-s currents of iPS cell-derived nociceptors. (A–F) Example recordings from a Ctrl 2 nociceptor explain the protocols used in voltage-clamp recordings on iPS cell-derived cells. (A) Shown is the prepulse protocol, used to eliminate space clamp artifacts in this particular Ctrl 2 neuron. The protocol consisted of a short prepulse (generally 4–6 ms,  $-50$  to  $-15$  mV), followed by a repolarizing interpulse (generally 1 ms,  $-120$  to  $-70$  mV), followed by the regular testpulse (40 ms,  $-80$  to  $+40$  mV, 10 mV increments). Prepulse and interpulse voltage and duration were adjusted to each cell individually to eliminate artefacts (F) and obtain optimal voltage-clamp conditions. When tested in  $\text{Na}_v1.7$ -expressing HEK293 cells, such prepulse protocols did not affect voltage dependence of activation of  $\text{Na}_v1.7$  and provided measurable current amplitudes during the testpulse (Supplementary Fig. S6, available at <http://links.lww.com/PAIN/A749>). (B) Total current measured in this particular neuron using the protocol shown in (A) before application of TTX. (C) TTX-resistant (TTX-r) current obtained from the same neuron after application of 500 nM TTX. (D) The TTX-sensitive (TTX-s) current component was calculated by subtracting the TTX-r current (C) from the total current (B). (E) Current–voltage (IV) relationships of the same neuron, obtained from the total current (black) shown in (B), the TTX-r current (blue) shown in (C), and the TTX-s current (red) shown in (D). The IV relationships confirm accurate voltage-clamp conditions, achieved by the prepulse protocol shown in (A). Incomplete inactivation of  $\text{Na}_v$ s during the interpulse (here  $-70$  mV) prevents current from reaching zero before the onset of the test pulse (see also B). (F) A regular voltage protocol without prepulse (40 ms,  $-80$  to  $+40$  mV, 10 mV increments) was run on the same neuron at the end of the recording after TTX had already been applied. The recorded TTX-r current shows bad voltage clamp and components from multiple cells, visible as delayed inward current peaks (red and blue with arrows). This confounds current–voltage analysis. iPS cell, induced pluripotent stem cell.

the mutation in  $\text{Na}_v1.7$  and is independent of other  $\text{Na}_v$  isoforms. Interestingly, the activation curve of IEM 2 nociceptors was only marginally different between recordings with and without ProTx-II application. By contrast, the activation curve of Ctrl 2 nociceptors was shifted significantly to hyperpolarized potentials when  $\text{Na}_v1.7$  was blocked (Figs. 6C and D). This suggests that in control nociceptors,  $\text{Na}_v1.7$  is responsible for a significant depolarization of the voltage dependence of activation.

Block of  $\text{Na}_v1.7$  also allowed us to measure the voltage dependence of all the remaining  $\text{Na}_v$  channels that are

expressed in these nociceptors (total current; including both TTX-s and TTX-r currents). Interestingly, the  $\text{Na}_v1.7$ -free total current in Ctrl 2 nociceptors also displayed a hyperpolarized activation compared with measurements where  $\text{Na}_v1.7$  was not blocked (Fig. 6E).

Taken together, these results demonstrate for the first time in human sensory neurons the predicted left shift of  $\text{Na}_v1.7$  activation induced by the  $\text{Na}_v1.7/1848\text{T}$  mutation. This shift not only affects the action potential threshold, but also particularly enhances the action potential upstroke and could

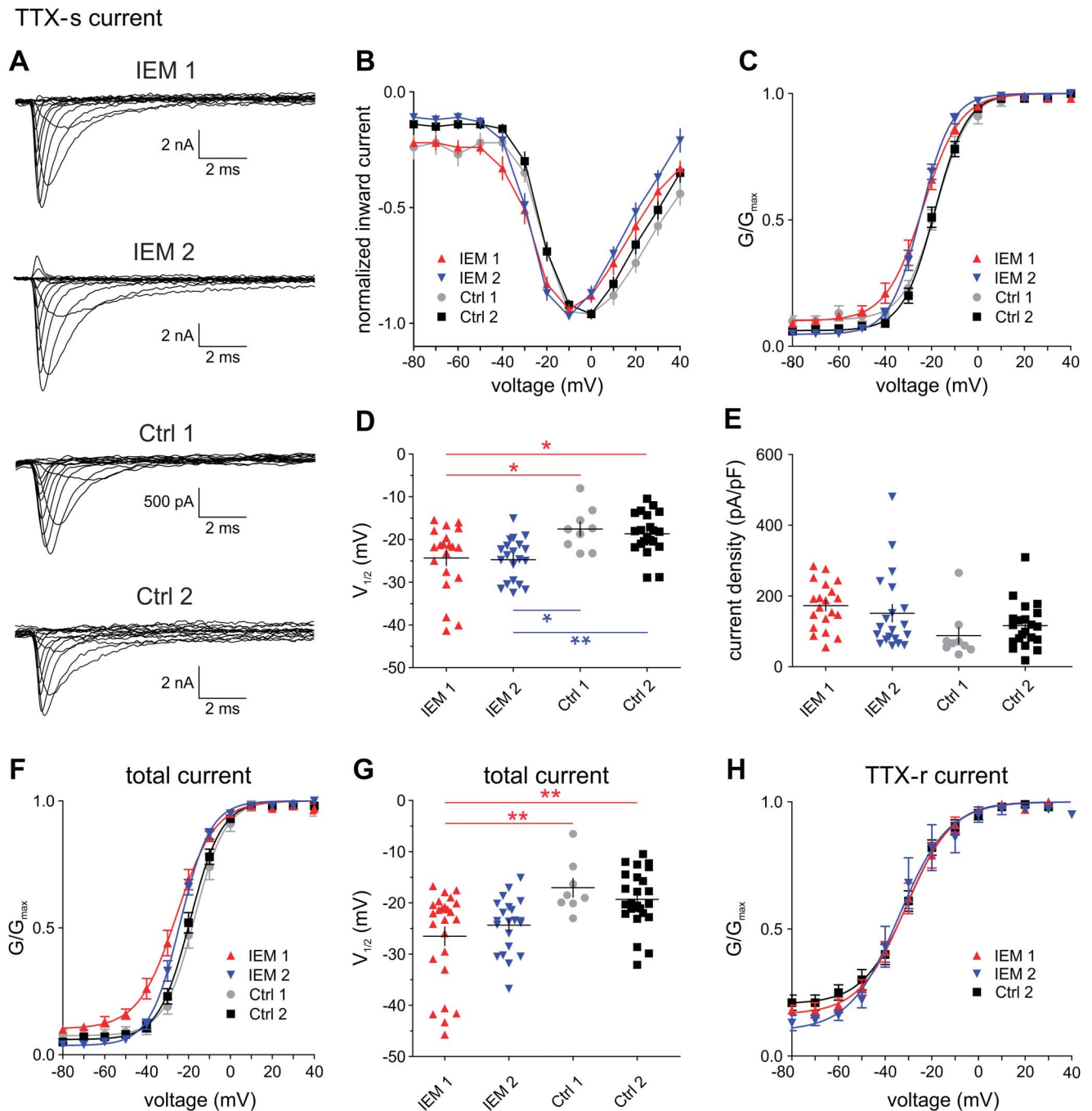


**Figure 5.** The IEM mutation hyperpolarizes the voltage dependence of activation. (A–E) Analysis of the voltage dependence of the TTX-s current component in iPS cell–derived nociceptors. (A) Example traces of TTX-s currents measured in nociceptors from the indicated clones. (B) Current–voltage relationship of TTX-s currents shows a left shift in both IEM clones. Current was normalized to the maximum inward current for each group. Due to the applied prepulse protocol, current does not start at 0.0 (Fig. 4). (C) Voltage dependence of activation of TTX-s currents obtained from data in (B). The left shift of the activation curves in both IEM clones is clearly visible. (D) Values for half-maximal voltage-dependent activation ( $V_{1/2}$ ) of TTX-s currents obtained from data in (C):  $-24.4 \pm 1.8$  mV for IEM 1 ( $P = 0.034$  vs Ctrl 1 and  $P = 0.018$  vs Ctrl 2),  $-24.7 \pm 1.1$  mV for IEM 2 ( $P = 0.021$  vs Ctrl 1 and  $P = 0.0099$  vs Ctrl 2),  $-17.6 \pm 1.6$  mV for Ctrl 1, and  $-18.7 \pm 1.1$  mV for Ctrl 2. (E) TTX-s current density showed no significant differences between different clones:  $173 \pm 15$  pA/pF for IEM 1,  $151 \pm 25$  pA/pF for IEM 2,  $88 \pm 24$  pA/pF for Ctrl 1, and  $116 \pm 14$  pA/pF for Ctrl 2 (all  $P \geq 0.07$ ). (F) Voltage dependence of activation of total currents, measured before application of TTX. The  $\text{Na}_v1.7$ -mediated left shift is discernible between IEM and Ctrl clones. (G)  $V_{1/2}$  values of total currents obtained from data in (F):  $-26.5 \pm 1.8$  mV for IEM 1 ( $P = 0.006$  vs Ctrl 1 and  $P = 0.002$  vs Ctrl 2),  $-24.4 \pm 1.2$  mV for IEM 2 ( $P = 0.073$  vs Ctrl 1 and  $P = 0.092$  vs Ctrl 2),  $-17 \pm 1.8$  mV for Ctrl 1, and  $-18.9 \pm 1.1$  mV for Ctrl 2. (H) Voltage dependence of activation of TTX-r currents. See Table 1 for all  $V_{1/2}$ , slope, current density, and  $n$  values. All 1-way ANOVA with Bonferroni multiple comparisons test. ANOVA, analysis of variance; IEM, inherited erythromalgia; iPS cell, induced pluripotent stem cell.

thereby lead to the increased pain phenotype of IEM patients. This study establishes human iPS cell–derived sensory neurons as a suitable model system to investigate the effect of  $\text{Na}_v$  channel mutations, not only by current-clamp but also by voltage-clamp electrophysiology. It should be noted,

however, that although the voltage-clamp results are comparable with those obtained in heterologous expression systems, the current-clamp results in these human sensory neurons differ substantially from recordings in rodent neurons, highlighting the importance of this translational model.

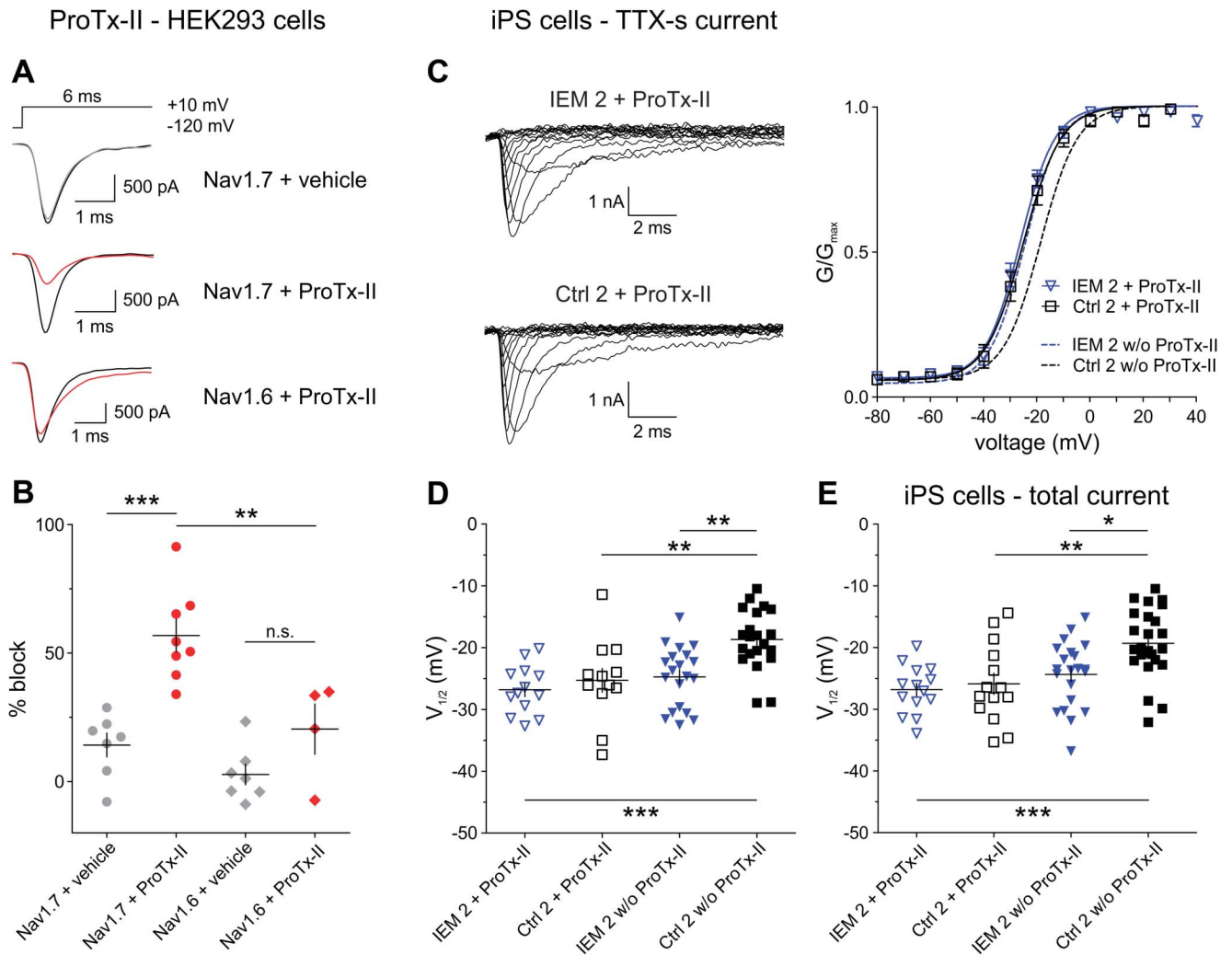


**Figure 6.** Block of  $Na_v1.7$  using ProTx-II reveals a hyperpolarized voltage dependence. (A) Representative traces displaying tonic block by 10 nM ProTx-II or vehicle in HEK293 cells, expressing  $Na_v1.7$  (upper and middle) or  $Na_v1.6$  (lower). Voltage protocol (above) was applied every 2 seconds for 10 minutes. (B) ProTx-II- or vehicle-mediated block in  $Na_v1.7$  and 1.6 expressing HEK293 cells. For  $Na_v1.7$ , vehicle and ProTx-II for 10 minutes reduced peak current by  $14.2 \pm 4.7\%$  and  $56.8 \pm 6.4\%$  ( $P = 0.0001$ ;  $n = 7$  and 8), respectively. For  $Na_v1.6$ , block was  $2.7 \pm 4\%$  for vehicle and  $20.4 \pm 9.8\%$  for ProTx-II ( $P = 0.45$  vs  $Na_v1.6$  + vehicle and  $P = 0.004$  vs  $Na_v1.7$  + ProTx-II;  $n = 7$  and 4). (C and D) Analysis of the TTX-s current component in iPS cell-derived nociceptors (IEM 2 and Ctrl 2) after incubation in 5 nM ProTx-II for  $\geq 10$  minutes. (C) Left: TTX-s currents with ProTx-II. Right: TTX-s voltage dependence of activation with ProTx-II (solid lines). For comparison, TTX-s curves without ProTx-II are presented with dashed lines (same as in Fig. 5C). Block of  $Na_v1.7$  induces a left shift of activation in control but not in IEM nociceptors. (D)  $V_{1/2}$  values of TTX-s currents with or without ProTx-II:  $-26.8 \pm 1.1$  mV (IEM 2) and  $-25.3 \pm 1.9$  mV (Ctrl 2) with ProTx-II ( $P = 0.99$ ).  $V_{1/2}$  values without ProTx-II are presented for comparison (same as in Fig. 5D) (IEM 2:  $-24.7 \pm 1.1$  mV,  $P = 0.99$  vs IEM 2 + ProTx-II; Ctrl 2:  $-18.7 \pm 1.1$  mV,  $P = 0.002$  vs IEM 2 w/o ProTx-II,  $P = 0.004$  vs Ctrl 2 + ProTx-II, and  $P = 0.0002$  vs IEM 2 + ProTx-II). (E) The total current also shows a left shift of activation in control neurons. For Ctrl 2,  $V_{1/2}$  was  $-25.9 \pm 1.7$  mV with ProTx-II, but  $-18.9 \pm 1.1$  mV without ProTx-II ( $P = 0.003$ ). For IEM 2,  $V_{1/2}$  was  $-26.8 \pm 1.1$  mV with ProTx-II and  $-24.4 \pm 1.2$  mV without ProTx-II ( $P = 0.99$  vs IEM 2 + ProTx-II,  $P = 0.015$  vs Ctrl 2 w/o ProTx-II). Values without ProTx-II are the same as in Fig. 5G. All 1-way ANOVA with Bonferroni multiple comparisons test. ANOVA, analysis of variance; IEM, inherited erythromelalgia; iPS cell, induced pluripotent stem cell.

#### 4. Discussion

Treatment of chronic pain conditions has remained unsatisfying over the past decades despite considerable advances in our molecular understanding of these diseases. A major obstacle in developing novel analgesic strategies has been the limited availability of human tissue and relevant translational assays. Here, we describe a human model system to investigate sensory neurons and their sodium channel function, which can be used to study mutation-linked pathomechanisms and to develop and validate disease-specific compounds. The human iPS cell-derived nociceptors reveal functional characteristics of adult sensory neurons. The molecular changes induced by the  $Na_v1.7$ /I848T-IEM mutation in rodent tissue are partly, but importantly not completely, mirrored in this human model system. Similar iPS

cell-derived nociceptors have been shown to express both TTX-s and TTX-r  $Na_v$  isoforms as well as other sensory neuron-specific ion channels,<sup>5,16,46</sup> which corresponds well with our results.

A recent study used iPS cell-derived nociceptors to investigate the effects of the  $Na_v1.7$ /I848T mutation in IEM patient neurons.<sup>5</sup> The authors mainly found an increase in spontaneous firing and a reduction of action potential rheobase. However, contrary to what has been shown in rodent neurons,<sup>19</sup> evoked action potential firing was not significantly increased in human iPS cell-derived neurons, comparable with our results. In addition, a novel  $Na_v1.7$  inhibitor provided only short-lasting pain relief in the I848T patient.<sup>5</sup> Thus, the study leaves a number of open questions: (1) How important is  $Na_v1.7$  in action potential generation? (2) Is the predicted hyperpolarized shift of  $Na_v1.7$ /I848T activation even present in human nociceptors? (3) Are the



observed changes in the I848T neurons pathophysiologically relevant? In this study, we addressed these questions by determining the voltage dependence of  $\text{Na}_v1.7$  in iPS cell-derived nociceptors for the first time and by investigating the contribution of  $\text{Na}_v1.7$  to action potential generation.

#### 4.1. Voltage sensitivity of activation is hyperpolarized in erythromelalgia nociceptors

The IEM-inducing  $\text{Na}_v1.7/\text{I848T}$  mutation has been predicted to cause a hyperpolarizing shift in the activation of  $\text{Na}_v1.7$ , leading to a reduced action potential threshold and consequently to increased pain sensation.<sup>11,19</sup> Our results confirm the predicted hyperpolarizing shift in the activation of  $\text{Na}_v1.7$  in human nociceptors and show that this shift does indeed lead to a reduced action potential threshold. The I848T mutation was reported to induce a 10 to 14 mV left shift of activation in heterologous expression systems.<sup>11,40</sup> We measured a 6.4 mV difference between IEM and control nociceptors. Given the fact that the IEM nociceptors investigated here carry a heterozygous mutation and therefore contain a combination of mutant  $\text{Na}_v1.7$  and unmutated channels, our results correlate very well with the previous reports.<sup>11,40</sup> The hyperpolarized shift was not only observed in the TTX-s current component but also in the total whole-cell current before application of TTX. This shows that the left shift of  $\text{Na}_v1.7$  activation is not compensated for by other channels or mechanisms but will most likely affect excitability in these nociceptors. Indeed, we observed a reduced action potential threshold of IEM nociceptors as compared to unmutated control cells.

Contrary to what has been predicted based on experiments in rodent sensory neurons,<sup>19</sup> we did not see a clear or consistent increase in firing frequency due to large variability. This is in line with the aforementioned study on patient iPS cell-derived nociceptors<sup>5</sup> and may indicate that increased action potential frequency is not necessarily a prerequisite for increased pain perception. However, tonic action potential firing was more pronounced in IEM nociceptors, possibly indicating a lack of activity-dependent inhibition or even activity-dependent increase in excitability that could lead to pain attacks. Contrary to the study by Cao et al.,<sup>5</sup> we did not find an increase in spontaneous action potential firing in our IEM nociceptors. The most likely explanations for this discrepancy are slight differences in the composition of differentiation and maturation media, which could affect ion channel expression. In addition, there are small differences in the ionic composition of the electrophysiological recording solutions between our study and the one by Cao et al. These small differences (mostly in the  $\text{K}^+$  gradient) lead to a small shift of the Nernst potential, thus potentially inducing changes in neuronal excitability.

We performed a detailed investigation of individual action potentials that revealed changes in several action potential characteristics induced by the IEM mutation: decreased threshold, increased amplitude, stronger afterhyperpolarization, as well as shorter and faster action potentials. Taken together, these findings suggest that due to the hyperpolarized voltage dependence,  $\text{Na}_v1.7/\text{I848T}$  channels open sooner and in a more synchronized manner. This lowers the action potential threshold, meaning that a weak, potentially nonnoxious stimulus is enough to induce action potentials and might even trigger a pain attack.

#### 4.2. $\text{Na}_v1.7$ plays a key role in action potential generation

It has previously been hypothesized that  $\text{Na}_v1.7$  is an amplifier of subthreshold stimuli, responsible for depolarizing the membrane potential to a point when  $\text{Na}_v1.8$  and  $1.6$  activate, which would

then carry the upstroke of the action potential.<sup>2,13,14,34</sup> Our results argue that  $\text{Na}_v1.7$  is unlikely to be a subthreshold channel because the slope of the subthreshold depolarization of the action potential is not changed in IEM nociceptors. In addition, blocking  $\text{Na}_v1.7$  by ProTx-II displayed a hyperpolarized voltage dependence of activation, suggesting that the remaining  $\text{Na}_v$  isoforms open before  $\text{Na}_v1.7$  and are therefore likely to carry subthreshold depolarizations. This corresponds well with published activation  $V_{1/2}$  values for these  $\text{Na}_v$  channels ( $\text{Na}_v1.1$ ,<sup>6,8</sup>  $\text{Na}_v1.2$ ,<sup>8,22,44</sup>  $\text{Na}_v1.3$ ,<sup>8,10</sup>  $\text{Na}_v1.6$ ,<sup>4,8,36</sup> and  $\text{Na}_v1.9$ <sup>26,41</sup>), all of which were reported to be more hyperpolarized compared with  $\text{Na}_v1.7$ .<sup>10,11,18,24,40,43</sup>

As outlined in **Figure 7**, we show that the action potential upstroke depends significantly on  $\text{Na}_v1.7$  activity: action potential amplitude is increased, time to peak of the action potential is decreased, and the slope of the action potential upstroke is increased in IEM nociceptors. In addition,  $\text{Na}_v1.7$  seems to be crucial for the setting of the action potential threshold because the hyperpolarizing IEM mutation significantly reduces the neuron's firing threshold. This concept is supported by previous pharmacological evidence demonstrating that a specific  $\text{Na}_v1.7$  inhibitor affected the action potential threshold and rising phase of the DRG action potential but not the subthreshold phase.<sup>1</sup>

In patients suffering from IEM, the hyperpolarized voltage sensitivity of  $\text{Na}_v1.7$  could lead to a more synchronized activation of different  $\text{Na}_v$  isoforms (**Fig. 7**). This would accelerate and increase the depolarization. As a result, it is possible that in IEM nociceptors, TTX-s isoforms other than  $\text{Na}_v1.7$  participate in the action potential upstroke. This increases the amplitude and the slope of the action potential. All these mechanisms together with the enhanced hyperpolarization support faster action potential propagation and potentially increased neurotransmitter release. These findings taken together argue that  $\text{Na}_v1.7$  is a key channel in defining action potential characteristics and in guaranteeing normal excitability of nociceptors. This crucial role of  $\text{Na}_v1.7$  is supported by the large number of mutations in  $\text{Na}_v1.7$  that are known to modify pain sensitivity in one way or another.<sup>15,17</sup>

#### 4.3. Erythromelalgia nociceptors display paradoxical activity-dependent speeding of conduction

In a previous study, we investigated conduction velocity of C-fiber nociceptors in an IEM patient carrying the same mutation using microneurography.<sup>30</sup> In C-fiber nociceptors of this patient, normal activity-dependent slowing of conduction was turned into activity-dependent speeding. Based on these data, we predicted that the latter effect could be due to a more pronounced afterhyperpolarization in the neurons expressing the I848T mutation.<sup>30</sup> This hypothesis is now confirmed in this study.

In that previous study, we also showed a slower resting conduction velocity in human IEM nociceptors *in vivo*.<sup>30</sup> This could be due to an increased amount of inactivated  $\text{Na}_v$ s at rest. Here, we show a slightly increased TTX-s  $\text{Na}_v$  activity at RMP in IEM nociceptors (more channels open around  $-40$  mV, **Fig. 5C**), which could lead to inactivation and therefore reduce conduction velocity. More importantly, the strongly enhanced hyperpolarization after an action potential in IEM nociceptors reverses this increased inactivation of resting TTX-s  $\text{Na}_v$ s, creating a positive feedback loop and leading to faster-than-normal conduction in the later phase after an action potential, thus supporting our previous hypothesis. Combining the results of our previous clinical study with the present stem cell-based cellular study, we suggest that patients carrying the  $\text{Na}_v1.7/\text{I848T}$  mutation suffer from increased pain sensation due to a reduced firing threshold in

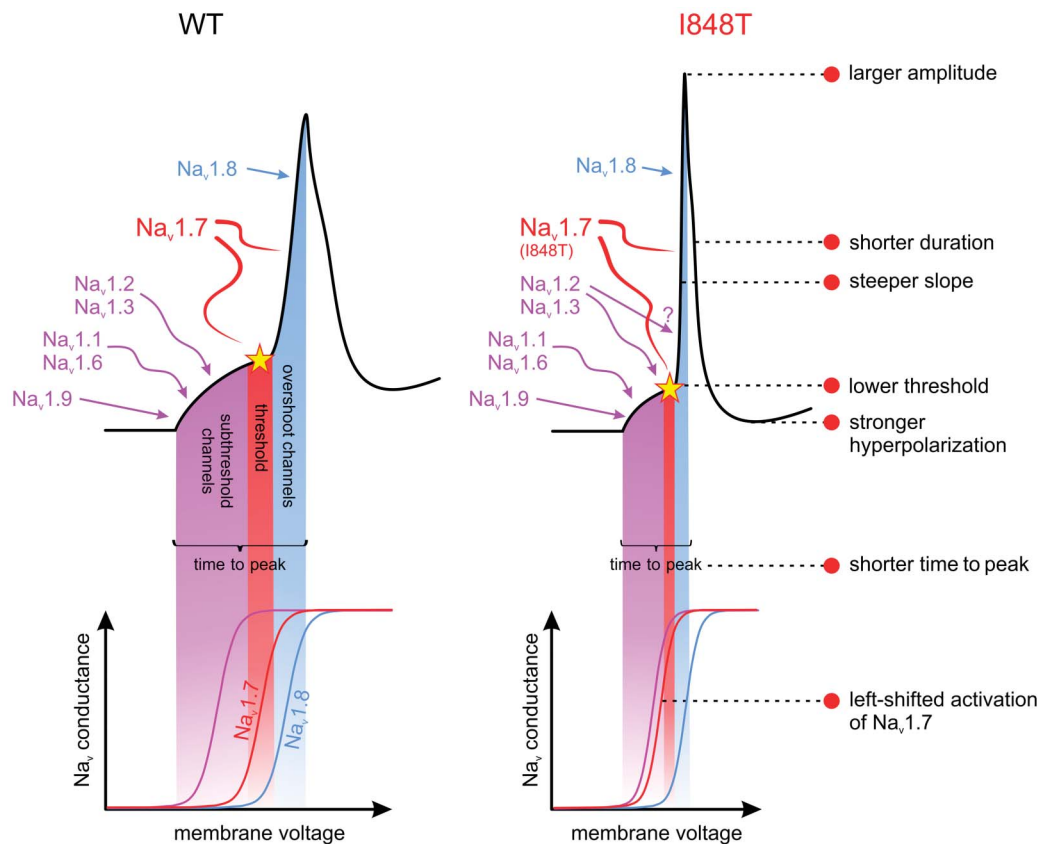


**Figure 7.** Proposed distribution of  $\text{Na}_v$  channels during action potential generation. Top: schematic representations of action potentials from wild-type (WT, left) or  $\text{Na}_v1.7/\text{I848T}$  (right) nociceptors. The individual phases of the action potential are shaded in different colors to match the assumed contribution of different  $\text{Na}_v$  isoforms to each particular phase. Bottom: schematic activation curves for the different  $\text{Na}_v$  channel categories, based on the data presented in this study. We propose that in the wild-type (left panel)  $\text{Na}_v1.1$ , 1.2, 1.3, 1.6, and 1.9 (purple) contribute mainly to subthreshold depolarizations because their voltage dependence is very hyperpolarized.  $\text{Na}_v1.7$  (red) has a more depolarized activation curve and defines the action potential threshold but also contributes to the upstroke.  $\text{Na}_v1.8$  (blue) with its very depolarized activation contributes mainly to the action potential upstroke. In patients carrying the IEM mutation  $\text{Na}_v1.7/\text{I848T}$  (right panel), activation of  $\text{Na}_v1.7$  is crucially shifted towards negative potentials. This leads to more synchronized activation of  $\text{Na}_v1.7$  and other TTX-s  $\text{Na}_v$ s (note the vicinity of the red and purple activation curves). This synchronized activity leads to a lowering of the action potential threshold and to a speeding up of the upstroke. It is possible that  $\text{Na}_v1.2$  and 1.3 now also contribute to the action potential upstroke in addition to  $\text{Na}_v1.7$  and 1.8. This further enhances slope and amplitude of the action potential upstroke. Taken together, action potentials in IEM ( $\text{I848T}$ ) patients are faster and larger and display particular changes, summarized on the right. Comparing the 2 graphs of activation curves (bottom panel), please note the shorter X-axis in the bottom right graph. We do not propose a shift of either the purple or the blue ( $\text{Na}_v1.8$ ) activation curve. IEM, inherited erythromelalgia.

combination with an activity-dependent increase of axonal excitability.

In summary, we show that the  $\text{Na}_v1.7/\text{I848T}$  mutation induces a hyperpolarized shift of voltage-dependent activation in a human patient-derived model system for IEM. This shift reduces the action potential threshold, enhances and speeds up the action potential upstroke, and increases hyperpolarization, inducing increased pain sensitivity in patients. These results from human nociceptors advance previous findings in human model systems and differ from previous reports on rodent sensory neurons, highlighting the impact of species differences. We therefore present iPS cell-derived neurons as a valuable tool for studying pain mechanisms and for developing and testing potential new pharmaceuticals. Finally, our results suggest a crucial role for  $\text{Na}_v1.7$  in action potential generation and propagation.

### Conflict of interest statement

A.M.R. and M.R. are shareholders and employees and M.R. is a founder and the director of Metrion Biosciences, Cambridge, United Kingdom. R.G. is an employee and W.W. is a cofounder of

Cygenia GmbH, Aachen, Germany. The remaining authors have no conflicts of interest to declare.

### Acknowledgements

The authors thank B. Hoch and U. Gollan for excellent technical assistance, and Jürgen Winkler and Sonja Plötz for culture of fibroblasts.

This work was supported in part by the Ministry for Innovation, Science and Research of the German Federal State of North Rhine-Westphalia, Duesseldorf, Germany (S.S. and M.Z.), by the Bavarian Ministry of Education and Culture, Science, and the Arts in the framework of the Bavarian Molecular Biosystems Research Network, ForIPS, and the DFG-funded research training group GRK2162 (B.W.), GRK2416 (A.L.), and SFB 1158 (M.S.), by the Johannes and Frieda Marohn-Foundation (Win/2012 to B.W. and A.L.), by the Excellence Initiative of the German federal and state governments (Dean's Seed Fund of the RWTH Aachen University, A.L.), by the German Israeli Foundation (GIF, 1091-27.1/2010 to A.L.), by a grant from the Interdisciplinary Center for Clinical Research within the faculty of medicine at the RWTH Aachen

University (B.N.), and the DFG grant NA 970 3 to 1 (B.N.) and LA 2740/3 to 1 (A.L.).

Author contributions: J.E. Meents planned and designed experiments, performed and analyzed patch-clamp experiments, interpreted the data, and wrote the manuscript. E. Bressan planned and designed experiments, generated and characterized iPS cells and iPS cell-derived neurons, performed and analyzed immunofluorescence and calcium imaging experiments, interpreted data, and contributed to writing the manuscript. S. Sontag planned and designed experiments, generated and characterized iPS cells, interpreted data, and wrote the manuscript. A. Foerster planned and designed experiments, performed and analyzed patch-clamp experiments, differentiated and maintained iPS cells, and contributed to writing the manuscript. P. Hautvast planned and designed experiments, performed and analyzed qPCR experiments, and differentiated and maintained iPS cells. C. Rösseler planned and designed experiments, and differentiated and maintained iPS cells. M. Hampl programmed analysis software for patch-clamp analysis, and supported design, analysis, and interpretation of patch-clamp experiments. H. Schüler performed and analyzed cytogenetic analysis. R. Goetzke performed Epi-Pluri-Score analysis. T.K.C. Le performed and analyzed patch-clamp experiments with ProTx-II, and interpreted data. I.P. Kleggetveit participated in assessment of the patients, took skin biopsies, and critically revised the manuscript. K. Le Cann performed current-clamp experiments and interpreted data. C. Kerth performed and analyzed patch-clamp experiments in HEK cells, and interpreted data. A.M. Rush discussed the results and critically revised the manuscript. M. Rogers discussed the results and critically revised the manuscript. Z. Kohl maintained fibroblast culture, helped to generate iPS cells, and interpreted data. M. Schmelz discussed the results and critically revised the manuscript. W. Wagner supported epigenetic characterization of iPS cells and critically revised the manuscript. E. Jorum is responsible for the recruitment of the IEM patients, their clinical assessment, and discussed data. B. Namer conceived the study, discussed experimental design, and critically revised the manuscript. B. Winner conceived the study, planned and designed experiments, and critically revised the manuscript. M. Zenke planned and designed experiments, interpreted data, and critically revised the manuscript. A. Lampert conceived the study, planned and designed experiments, analyzed and interpreted the data, and participated in writing and critically revising the manuscript.

## Appendix A. Supplemental digital content

Supplemental digital content associated with this article can be found online at <http://links.lww.com/PAIN/A749>.

### Article history:

Received 13 September 2018

Received in revised form 9 January 2019

Accepted 25 January 2019

Available online 22 March 2019

## References

- Alexandrou AJ, Brown AR, Chapman ML, Estacion M, Turner J, Mis MA, Wilbrey A, Payne EC, Gutteridge A, Cox PJ, Doyle R, Printzenhoff D, Lin Z, Marron BE, West C, Swain NA, Storer RI, Stuppel PA, Castle NA, Hounshell JA, Rivara M, Randall A, Dib-Hajj SD, Krafte D, Waxman SG, Patel MK, Butt RP, Stevens EB. Subtype-selective small molecule inhibitors reveal a fundamental role for Nav1.7 in nociceptor electrogenesis, axonal conduction and presynaptic release. *PLoS One* 2016;11:e0152405.
- Blair NT, Bean BP. Roles of tetrodotoxin (TTX)-sensitive Na<sup>+</sup> current, TTX-resistant Na<sup>+</sup> current, and Ca<sup>2+</sup> current in the action potentials of nociceptive sensory neurons. *J Neurosci* 2002;22:10277–90.
- Blanchard JW, Eade KT, Szűcs A, Lo Sardo V, Tsunemoto RK, Williams D, Sanna PP, Baldwin KK. Selective conversion of fibroblasts into peripheral sensory neurons. *Nat Neurosci* 2015;18:25–35.
- Burbidge SA, Dale TJ, Powell AJ, Whitaker WRJ, Xie XM, Romanos MA, Clare JJ. Molecular cloning, distribution and functional analysis of the NAV1.6. Voltage-gated sodium channel from human brain. *Mol Brain Res* 2002;103:80–90.
- Cao L, McDonnell A, Nitzsche A, Alexandrou A, Saintot PP, Loucif AJC, Brown AR, Young G, Mis M, Randall A, Waxman SG, Stanley P, Kirby S, Tarabar S, Gutteridge A, Butt R, McKernan RM, Whiting P, Ali Z, Bilsland J, Stevens EB. Pharmacological reversal of a pain phenotype in iPSC-derived sensory neurons and patients with inherited erythromelalgia. *Sci Transl Med* 2016;8:335ra56.
- Cestèle S, Scalmani P, Rusconi R, Terragni B, Franceschetti S, Mantegazza M. Self-limited hyperexcitability: functional effect of a familial hemiplegic migraine mutation of the Nav1.1 (SCN1A) Na<sup>+</sup> channel. *J Neurosci* 2008;28:7273–83.
- Chambers SM, Qi Y, Mica Y, Lee G, Zhang XJ, Niu L, Bilsland J, Cao L, Stevens E, Whiting P, Shi SH, Studer L. Combined small-molecule inhibition accelerates developmental timing and converts human pluripotent stem cells into nociceptors. *Nat Biotechnol* 2012;30:715–20.
- Clare JJ. Current approaches for the discovery of novel NaV channel inhibitors for the treatment of brain disorders. In: Parnham PMJ, Coward K, Baker MD, editors. *Sodium channels, pain, and analgesia. progress in inflammation research*. Basel: Birkhäuser, 2005. p. 23–62. doi:10.1007/3-7643-7411-X\_2.
- Cox JJ, Reimann F, Nicholas AK, Thornton G, Roberts E, Springell K, Karbani G, Jafri H, Mannan J, Raashid Y, Al-Gazali L, Hamamy H, Valente EM, Gorman S, Williams R, McHale DP, Wood JN, Gribble FM, Woods CG. An SCN9A channelopathy causes congenital inability to experience pain. *Nature* 2006;444:894–8.
- Cummins TR, Aglieco F, Renganathan M, Herzog RI, Dib-Hajj SD, Waxman SG. Nav1.3 sodium channels: rapid repriming and slow closed-state inactivation display quantitative differences after expression in a mammalian cell line and in spinal sensory neurons. *J Neurosci* 2001;21:5952–61.
- Cummins TR, Dib-Hajj SD, Waxman SG. Electrophysiological properties of mutant Nav1.7 sodium channels in a painful inherited neuropathy. *J Neurosci* 2004;24:8232–6.
- Cummins TR, Howe JR, Waxman SG. Slow closed-state inactivation: a novel mechanism underlying ramp currents in cells expressing the hNE/PN1 sodium channel. *J Neurosci* 1998;18:9607–19.
- Dib-Hajj SD, Geha P, Waxman SG. Sodium channels in pain disorders: pathophysiology and prospects for treatment. *PAIN* 2017;158:S97–S107.
- Dib-Hajj SD, Waxman SG. Diversity of composition and function of sodium channels in peripheral sensory neurons. *PAIN* 2015;156:2406–7.
- Dib-Hajj SD, Yang Y, Black JA, Waxman SG. The Nav1.7 sodium channel: from molecule to man. *Nat Rev Neurosci* 2013;14:49–62.
- Eberhardt E, Havlicek S, Schmidt D, Link AS, Neacsu C, Kohl Z, Hampl M, Kist AM, Klinger A, Nau C, Schüttler J, Alzheimer C, Winkler J, Namer B, Winner B, Lampert A. Pattern of functional TTX-resistant sodium channels reveals a developmental stage of human iPSC- and ESC-derived nociceptors. *Stem Cell Rep* 2015;5:305–13.
- Emery EC, Habib AM, Cox JJ, Nicholas AK, Gribble FM, Woods CG, Reimann F. Novel SCN9A mutations underlying extreme pain phenotypes: unexpected electrophysiological and clinical phenotype correlations. *J Neurosci* 2015;35:7674–81.
- Hampl M, Eberhardt E, O'Reilly AO, Lampert A. Sodium channel slow inactivation interferes with open channel block. *Sci Rep* 2016;6:25974.
- Han C, Dib-Hajj SD, Lin Z, Li Y, Eastman EM, Tyrrell L, Cao X, Yang Y, Waxman SG. Early- and late-onset inherited erythromelalgia: genotype–phenotype correlation. *Brain* 2009;132:1711–22.
- Han C, Estacion M, Huang J, Vasylyev D, Zhao P, Dib-Hajj SD, Waxman SG. Human Na(v)1.8: enhanced persistent and ramp currents contribute to distinct firing properties of human DRG neurons. *J Neurophysiol* 2015;113:3172–85.
- Herzog RI, Cummins TR, Ghassemi F, Dib-Hajj SD, Waxman SG. Distinct repriming and closed-state inactivation kinetics of Nav1.6 and Nav1.7 sodium channels in mouse spinal sensory neurons. *J Physiol* 2003;551:741–50.
- Kamiya K, Kaneda M, Sugawara T, Mazaki E, Okamura N, Montal M, Makita N, Tanaka M, Fukushima K, Fujiwara T, Inoue Y, Yamakawa K. A



- nonsense mutation of the sodium channel gene SCN2A in a patient with intractable epilepsy and mental decline. *J Neurosci* 2004;24:2690–8.
- [23] Lampert A, Eberhardt M, Waxman SG. Altered sodium channel gating as molecular basis for pain: contribution of activation, inactivation, and resurgent currents. In: Ruben PC, editor. *Voltage gated sodium channels. Handbook of experimental pharmacology*. Berlin: Springer, 2014. p. 91–110. Available at: [http://link.springer.com/chapter/10.1007/978-3-642-41588-3\\_5](http://link.springer.com/chapter/10.1007/978-3-642-41588-3_5). Accessed September 24, 2014.
- [24] Lampert A, O'Reilly AO, Dib-Hajj SD, Tyrrell L, Wallace BA, Waxman SG. A pore-blocking hydrophobic motif at the cytoplasmic aperture of the closed-state Nav1.7 channel is disrupted by the erythromelalgia-associated F1449V mutation. *J Biol Chem* 2008;283:24118–27.
- [25] Lenz M, Goetzke R, Schenk A, Schubert C, Veeck J, Herneda H, Koschmieder S, Zenke M, Schuppert A, Wagner W. Epigenetic biomarker to support classification into pluripotent and non-pluripotent cells. *Sci Rep* 2015;5:8973.
- [26] Lin Z, Santos S, Padilla K, Printzenhoff D, Castle NA. Biophysical and pharmacological characterization of Nav1.9 voltage dependent sodium channels stably expressed in HEK-293 cells. *PLoS One* 2016;11:e0161450.
- [27] Middleton RE, Warren VA, Kraus RL, Hwang JC, Liu CJ, Dai G, Brochu RM, Kohler MG, Gao YD, Garsky VM, Bogusky MJ, Mehl JT, Cohen CJ, Smith MM. Two tarantula peptides inhibit activation of multiple sodium channels. *Biochemistry* 2002;41:14734–47.
- [28] Milesco LS, Bean BP, Smith JC. Isolation of somatic Na<sup>+</sup> currents by selective inactivation of axonal channels with a voltage prepulse. *J Neurosci* 2010;30:7740–8.
- [29] Minett MS, Pereira V, Sikandar S, Matsuyama A, Lollignier S, Kanellopoulos AH, Mancini F, Iannetti GD, Bogdanov YD, Santanavarela S, Millet Q, Baskozos G, MacAllister R, Cox JJ, Zhao J, Wood JN. Endogenous opioids contribute to insensitivity to pain in humans and mice lacking sodium channel Na<sub>v</sub>1.7. *Nat Commun* 2015;6:8967.
- [30] Namer B, Ørstavik K, Schmidt R, Kleggetveit IP, Weidner C, Mørk C, Kvernebo MS, Kvernebo K, Salter H, Carr TH, Segerdahl M, Quiding H, Waxman SG, Handwerker HO, Torebjörk HE, Jørum E, Schmelz M. Specific changes in conduction velocity recovery cycles of single nociceptors in a patient with erythromelalgia with the I848T gain-of-function mutation of Nav1.7. *PAIN* 2015;156:1637–46.
- [31] Nassar MA, Stirling LC, Forlani G, Baker MD, Matthews EA, Dickenson AH, Wood JN. Nociceptor-specific gene deletion reveals a major role for Nav1.7 (PN1) in acute and inflammatory pain. *Proc Natl Acad Sci U S A* 2004;101:12706–11.
- [32] Prè D, Nestor MW, Sproul AA, Jacob S, Koppensteiner P, Chinchalongporn V, Zimmer M, Yamamoto A, Noggle SA, Arancio O. A time course analysis of the electrophysiological properties of neurons differentiated from human induced pluripotent stem cells (iPSCs). *PLoS One* 2014;9:e103418.
- [33] Qin J, Sontag S, Lin Q, Mitzka S, Leisten I, Schneider RK, Wang X, Jauch A, Peitz M, Brüstle O, Wagner W, Zhao RC, Zenke M. Cell fusion enhances mesendodermal differentiation of human induced pluripotent stem cells. *Stem Cell Dev* 2014;23:2875–82.
- [34] Renganathan M, Cummins TR, Waxman SG. Contribution of Na<sub>v</sub>1.8 sodium channels to action potential electrogenesis in DRG neurons. *J Neurophysiol* 2001;86:629–40.
- [35] Rostock C, Schrenk-Siemens K, Pohle J, Siemens J. Human vs. mouse nociceptors—similarities and differences. *Neuroscience* 2017;387:13–27.
- [36] Royeck M, Horstmann MT, Remy S, Reitze M, Yaari Y, Beck H. Role of axonal Nav1.6 sodium channels in action potential initiation of CA1 pyramidal neurons. *J Neurophysiol* 2008;100:2361–80.
- [37] Rush AM, Dib-Hajj SD, Liu S, Cummins TR, Black JA, Waxman SG. A single sodium channel mutation produces hyper- or hypoexcitability in different types of neurons. *Proc Natl Acad Sci U S A* 2006;103:8245–50.
- [38] Schmalhofer WA, Calhoun J, Burrows R, Bailey T, Kohler MG, Weinglass AB, Kaczorowski GJ, Garcia ML, Koltzenburg M, Priest BT. ProTx-II, a selective inhibitor of Nav1.7 sodium channels, blocks action potential propagation in nociceptors. *Mol Pharmacol* 2008;74:1476–84.
- [39] Shields SD, Deng L, Reese RM, Dourado M, Tao J, Foreman O, Chang JH, Hackos DH. Insensitivity to pain upon adult-onset deletion of Nav1.7 or its blockade with selective inhibitors. *J Neurosci* 2018;38:10180–201.
- [40] Theille JW, Jarecki BW, Piekarz AD, Cummins TR. Nav1.7 mutations associated with paroxysmal extreme pain disorder, but not erythromelalgia, enhance Navβ4 peptide-mediated resurgent sodium currents. *J Physiol* 2011;589:597–608.
- [41] Vanoye CG, Kunic JD, Ehring GR, George AL. Mechanism of sodium channel Nav1.9 potentiation by G-protein signaling. *J Gen Physiol* 2013;141:193–202.
- [42] Wainger BJ, Buttermore ED, Oliveira JT, Mellin C, Lee S, Saber WA, Wang AJ, Ichida JK, Chiu IM, Barrett L, Huebner EA, Bilgin C, Tsujimoto N, Brenneis C, Kapur K, Rubin LL, Eggan K, Woolf CJ. Modeling pain *in vitro* using nociceptor neurons reprogrammed from fibroblasts. *Nat Neurosci* 2015;18:17–24.
- [43] Wu MT, Huang PY, Yen CT, Chen CC, Lee MJ. A novel SCN9A mutation responsible for primary erythromelalgia and is resistant to the treatment of sodium channel blockers. *PLoS One* 2013;8:e55212.
- [44] Xie X, Dale TJ, John VH, Cater HL, Peakman TC, Clare JJ. Electrophysiological and pharmacological properties of the human brain type IIA Na<sup>+</sup> channel expressed in a stable mammalian cell line. *Pflugers Arch* 2001;441:425–33.
- [45] Yang Y, Wang Y, Li S, Xu Z, Li H, Ma L, Fan J, Bu D, Liu B, Fan Z, Wu G, Jin J, Ding B, Zhu X, Shen Y. Mutations in SCN9A, encoding a sodium channel alpha subunit, in patients with primary erythromelalgia. *J Med Genet* 2004;41:171–4.
- [46] Young GT, Gutteridge A, Fox HD, Wilbrey AL, Cao L, Cho LT, Brown AR, Benn CL, Kammonen LR, Friedman JH, Bictash M, Whiting P, Bilsland JG, Stevens EB. Characterizing human stem cell-derived sensory neurons at the single-cell level reveals their ion channel expression and utility in pain research. *Mol Ther* 2014;22:1530–43.
- [47] Zhang X, Priest BT, Belfer I, Gold MS. Voltage-gated Na<sup>+</sup> currents in human dorsal root ganglion neurons. *eLife* 2017;6:e23235.
- [48] Zhang Z, Schmelz M, Segerdahl M, Quiding H, Centerholt C, Juréus A, Carr TH, Whiteley J, Salter H, Kvernebo MS, Ørstavik K, Helås T, Kleggetveit IP, Lunden LK, Jørum E. Exonic mutations in SCN9A (Nav1.7) are found in a minority of patients with erythromelalgia. *Scand J Pain* 2014;5:217–25.